CMB Data Analysis

Paniez Paykari & Jean-Luc Starck
Laboratoire AIM, CEA/DSM-CNRS-Universite Paris Diderot,
IRFU/SEDI-SAP, CEA Saclay,
Orme des Merisiers, 91191 Gif-sur-Yvette, France

August 5, 2011

Contents

1 Introduction to CMB Cosmology

About $400,000$ years after the big bang the temperature of the Universe fell to about a few thousand degrees. As a result the previously free electrons and protons combined and the Universe became neutral. This released a radiation which we now observe as the cosmic microwave background (CMB). The tiny fluctuations[1] in the temperature and polarization of the CMB carry a wealth of cosmological information. These so-called temperature anisotropies were predicted as the imprints of the initial density perturbations which gave rise to the present large-scale structures such as galaxies and clusters of galaxies. This relation between the present-day Universe and its initial conditions has made the CMB radiation one of the most preferred tools to understand the history of the Universe. The CMB radiation was discovered by radio astronomers Arno Penzias and Robert Wilson in 1965 [72] and earned them the 1978 Nobel Prize. This discovery was in support of the big bang theory and ruled out the only other available theory at that time — the steady state theory. The crucial observations of the CMB radiation were made by the Far-Infrared Absolute Spectrophotometer (FIRAS) instrument on the Cosmic Background Explorer (COBE) satellite [86] — orbited in 1989 – 1996. COBE made the most accurate measurements of the CMB frequency spectrum and confirmed it as being a black body to within experimental limits. This made the CMB spectrum the most precisely measured black body spectrum in nature. The CMB has a thermal black body spectrum at a temperature of 2.725 K: the spectrum peaks in the microwave range frequency of 160.2 GHz, corresponding to a 1.9 mm wavelength. The results of COBE inspired a series of ground- and balloon-based experiments, which measured CMB anisotropies on smaller scales over the next decade. During the 1990s, the first acoustic peak of the CMB power spectrum (see Figure 1) was measured with increasing sensitivity and by 2000 the BOOMERanG experiment [26] reported that the highest power fluctuations occur at scales of about one degree. A number of ground-based interferometers provided measurements of the fluctuations with higher accuracy over the next three years, including the Very Small Array [16], Degree Angular Scale Interferometer (DASI) [61] and the Cosmic Background Imager (CBI) [78]. DASI was the first to detect the polarization of the CMB and the CBI provided the first E-mode polarization spectrum with compelling evidence that it is out of phase with the T-mode spectrum.

In June 2001, NASA launched its second CMB mission (after COBE), Wilkinson Microwave Anisotropy Explorer (WMAP) [44], to make much more precise measurements of the CMB sky. WMAP measured the differences in the CMB temperature across the sky creating a full-sky map of the CMB in five different frequency bands. The mission also measured the CMB's E-mode and the foreground polarization. As of October 2010, the WMAP spacecraft has ended its mission after nine years of operation. Although WMAP provided very accurate measurements of the large angular-scale fluctuations in the CMB, it did not have the angular resolution to cover the smaller scale fluctuations which had been observed by previous ground-based interferometers. A third space mission, the Planck Surveyor [1], was launched by ESA[2] in May 2009 to measure the CMB on smaller scales than WMAP, as well as making precise measurements of the polarization of CMB. Planck represents an advance over WMAP in several respects: it observes in higher resolution, hence allowing one to probe the CMB power spectrum to smaller scales; it has a higher sensitivity and observes in nine frequency bands rather than five, hence improving the astrophysical foreground models. The mission has a wide variety of scientific aims, including: 1. detecting the total intensity/polarization of the primordial CMB anisotropies; 2. creating a galaxy-cluster cata-

[1]These tiny fluctuations are of the order of $O(10^{-5})$ and $O(10^{-7})$ for temperature and polarization respectively.
[2]http://www.esa.int/SPECIALS/Planck/index.html

logue through the Sunyaev-Zel'dovich (SZ) effect [93]; 3. observing the gravitational lensing of the CMB and the integrated Sachs Wolfe (ISW) effect [82]; 4. observing bright extragalactic radio and infrared sources; 5. observing the local interstellar medium, distributed synchrotron emission and the galactic magnetic field; 6. studying the local Solar System (planets, asteroids, comets and the zodiacal light). Planck is expected to yield data on a number of astronomical issues by 2012. It is thought that Planck measurements will mostly be limited by the efficiency of foreground removal, rather than the detector performance or duration of the mission − this is particularly important for the polarization measurements.

Technological developments over the past two decades have accelerated the progress in observational cosmology. The interplay between the new theoretical ideas and new observational data has taken cosmology from a purely theoretical domain into a field of rigorous experimental science and we are now in what is called the precision cosmology era. The CMB measurements have made the inflationary big bang theory the standard model of the early Universe. This theory predicts a roughly Gaussian distribution for the initial conditions of the Universe. The power spectrum of these fluctuations agrees well with the observations, although certain observables, such as the overall amplitude of the fluctuations, remain as free parameters of the cosmic inflation model.

Temperature and Polarization Power Spectrum

The observable quantity is the temperature of the CMB, which can be described as

$$T(\hat{p}) = T_{CMB}[1 + \Theta(\hat{p})] , \tag{1}$$

where $\Theta(\hat{p})$ is the temperature anisotropy in direction $\hat{p}$. This temperature field is expanded on the spherical harmonic functions with coefficients $a_{\ell m}$

$$\Theta(\hat{p}) = \sum_{\ell m} a_{\ell m} Y_{\ell m}(\hat{p}) , \tag{2}$$

where ℓ is the multipole moment, which is related to the angular size on the sky via $\ell \sim 180^\circ/\theta$, and m is the phase ranging from $-\ell$ to ℓ. For a Gaussian random field the average and variance carry all the information of the field. In case of $a_{\ell m}$, the average vanishes and the variance is given by

$$\langle a_{\ell m} a^*_{\ell' m'} \rangle = \delta_{\ell\ell'} \delta_{mm'} C_\ell , \tag{3}$$

where C_ℓ is called the CMB angular power spectrum and it only depends on ℓ due to the isotropy assumption. This spectrum depends on the cosmological parameters through an angular transfer function $T(k, \ell)$ as

$$C_\ell = 4\pi \int \frac{dk}{k}\, T^2(k, \ell) P(k) , \tag{4}$$

where k defines the scale and $P(k)$ is the primordial power spectrum (defining the initial conditions of the Universe). Up to 1996, the angular transfer function was calculated by solving a series of coupled Boltzmann equations simultaneously — a very time consuming process. In 1996 Seljak and Zaldarriaga [83] devised a new method for the calculation of this transfer function, improving its speed greatly — this is exactly what codes like the CMBFast [83] and CAMB [63] are based on.

The CMB power spectrum is what is used to estimate the cosmological parameters and hence accurate measurements of this spectrum from CMB experiments is the main goal of any CMB data

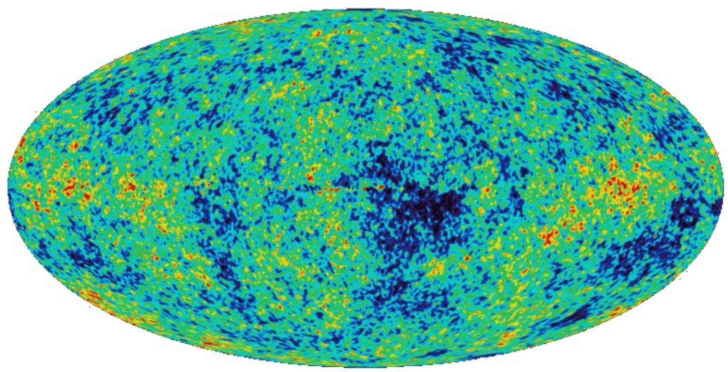

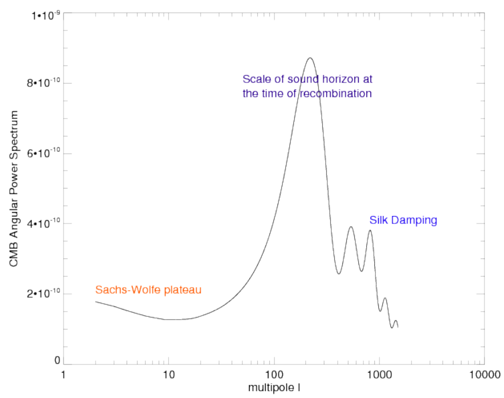

Figure 1: Top: CMB map seen by WMAP (*http://map.gsfc.nasa.gov/*). Bottom: CMB Angular Power Spectrum, showing the important scales discussed in the text.

analysis. The shape of the angular power spectrum is related to the physics of the oscillations of photons in the photon-baryon fluid at the time of recombination. The relative height and position of the peaks and troughs of the spectrum are of great importance as they are a direct impact of the cosmological parameters measured. For example, the first peak corresponds to the horizon scale at the time of recombination. It shows how far radiation has travelled since the big bang until the time of recombination. At angular scales above ten degrees ($\ell \lesssim 20$) main source of fluctuations is the Sachs Wolfe effect [82]. This effect is due to the gravitational redshift of the CMB photons causing the CMB spectrum to appear uneven. Also information about the present day galaxies can be obtained by Silk damping on angular scales $\ell \gtrsim 1000$. The Silk scale corresponds to the size of galaxies of the present day. Hence every aspect of the spectrum carries an important piece of information about cosmology and this reflects on the importance of the accurate measurements of this spectrum from CMB experiments.

Apart from the temperature anisotropy, the CMB radiation is polarized. This polarization is due to the Compton scattering at the time of recombination which thermalizes the CMB radiation. Therefore, there are three types of $a_{\ell m}$; a^E, a^B and a^T (E-mode, B-mode and temperature respectively), which can form six types of power spectra

$$\left\langle a_{\ell m}^{X} a_{\ell' m'}^{Y} \right\rangle = \delta_{\ell\ell'} \delta_{mm'} C_\ell^{XY} \ , \tag{5}$$

where $X, Y \in \{T, B, E\}$. The C_ℓ^{TT} power spectrum is the temperature power spectrum obtained previously. We expect $C_\ell^{BE} = C_\ell^{BT} = 0$ as any correlation between B and T/E would correspond to parity violation at recombination. The decomposition into E and B modes are particularly helpful because scalar/density fluctuations cannot produce B modes (B modes are only produced by directed quantities such as gravitational waves or lensing). Hence a B type detection is a direct signature of the presence of a stochastic background of gravitational waves. This would provide an invaluable information about inflation.

2 The CMB Data Analysis Pipeline

As explained previously the aim of all the CMB experiments is to estimate the cosmological parameters. Figure 2 shows a schematic illustration of the steps involved in estimating the cosmological parameters from CMB experiments. Each step involves a compression of information and hence the best techniques at each step are the ones with the least information loss. Below, we will go through the different steps shown in the Figure. Needless to say that this review may not do full justice to much of the work which has been done on this topic over the years. Nonetheless, we have tried to cover as much as possible, space permitting, and at least mention all the exciting work even if all the details are not fully covered. You can also refer to [22] for shorter review on the CMB data analysis.

2.1 From Raw to Time Ordered Data

The raw measured data from the satellite are pre-processed, cleaned (e.g., by removing glitches such as cosmic ray hits) and checked for any systematic problems. Each detecter's time stream noise correlation is characterized. The result of processing the raw data is the time-ordered data set (TOD), which is simply a list of the positions and temperatures of all the pixels observed, in chronological order. For single-difference experiments, such as WMAP, the TOD consists of pairs of pixel positions and temperature difference. For more general chopping schemes, each temperature in the TOD is some linear combination of the temperature across the sky. In principle, the cosmological parameters can be measured with the smallest error bars possible by performing a brute force likelihood analysis on the TOD. However, in practice, this is numerically unfeasible for large data sets and hence an intermediate step of reducing the TOD to sky maps and then a power spectrum is necessary.

2.2 Map-making

The map-making process passes the cosmological information from the TOD into a much smaller data set, the map. The best map-making method should retain all the cosmological information from the TOD so that the parameters can be measured just as accurately from the map(s) as from the full TOD. By linearity, the TOD data can be written as

$$d_t = s_t + n_t = A_{tp} s_p + n_t \ , \tag{6}$$

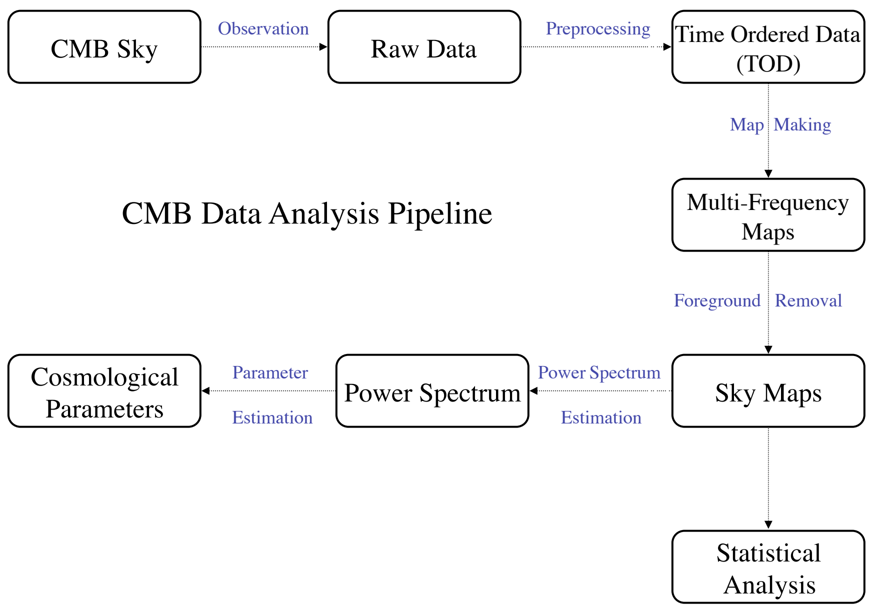

Figure 2: CMB data analysis pipeline.

where s_p is the temporally constant (but spatially varying) CMB signal and n_t is the temporal detector noise. The matrix A_{tp} is the pointing matrix which gives the weight of each pixel p in time sample t. This matrix is typically very sparse with normally only one nonzero entry for a total power temperature observation, two nonzero entries for a differencing temperature observation and three nonzeros for a total power polarization observation; the nonzero values in the rows correspond to the pixels being observed, at the time denoted by the row, and the columns, that typically have many nonzero entries, correspond to all the times a given pixel has been observed. The Gaussian noise likelihood function can be maximized over all possible sky signals to yield the map-making equations

$$N_{pp'}^{-1} = A_{tp}^T N_{tt'}^{-1} A_{t'p'} \ , \tag{7}$$

$$z_p = A_{tp}^T N_{tt'}^{-1} d_{t'} \ , \tag{8}$$

$$d_p = N_{pp'} z_{p'} \ . \tag{9}$$

This results in the sky maps for the different frequencies, where each frequency map is the weighted average of all the maps of the different channels at that frequency. One of the advantages of map-making is that it enables inclusion of maps at additional frequencies from other experiments. Generally, a Planck sky map will have $\sim 10^8$ pixels, while a WMAP map has $\sim 10^7$ pixels.

2.3 From Multichannel Maps to Cosmological Parameters

In the CMB experiments, as in many astrophysical observations, signals contain contributions from several components or sources. In efficiently designing experiments one aims to maximize the ability to subtract foregrounds and minimize the susceptibility to systematic errors. For example, incomplete sky coverage increases the sample variance (by a factor of about $1/\sqrt{\text{Covered Area}}$) and smears out features in the power spectrum. Therefore, one needs to choose an area such that the S/N per resolution element is of the order of unity or greater. Also, avoiding regions narrower than a few degrees in the smallest direction is helpful as a cold dark matter (CDM) spectrum has information on scales of order $\Delta_\ell = 30$.

Generally, the foregrounds are classified into three categories; diffuse galactic emission, extragalactic sources and solar system emission. The main emission mechanisms from our own galaxy are synchrotron radiation, free-free emission (lower frequencies) and astrophysical dust emissions (higher frequencies). The synchrotron emission is due to the relativistic electrons being accelerated in the galactic magnetic field. The free-free emission comes from the thermal bremsstrahlung that is caused by the acceleration of hot electrons in the interstellar gas. The observed dust emission is the total emission from all the dust grains along the line of sight. The extragalactic emissions include extragalactic sources, point sources and clusters of galaxies. To remove the foreground contamination in the CMB data, one can use prior information of the foreground signals to reduce their impact on the data: 1. For all-sky experiments the regions suspected to have significant foreground emissions are masked; for localized components in real space (like the galactic plane) one can discard or down-weigh the polluted regions. The drawbacks, however, are the resulting incomplete sky maps. 2. For ground-based/balloon-borne experiments one would observe in the regions where the contamination is minimal, for example in directions away from the galactic plane. 3. The CMB itself dominates at a frequency of $\sim 70 - 100$ GHz, but for an efficient component separation a range of channels needs to be observed. Note that ground-based observations are limited by the frequency window permitted by the atmosphere. Based on the observations made at the different frequencies, an estimate of the foreground emissions can be obtained and subtracted from the observations. This procedure is very model-dependent but can help reduce the amount of cut sky.

Component separation consists of estimating a set of parameters which describe the components of interest. For example, it could be parameters describing the statistical properties such as power spectra and spectral indices. However, this is very difficult in practice and there are many methods that have been developed in order to recover the CMB from the multichannel data. The main difficulties are;

- The noise is not stationary as different sections of the sky are observed different number of times, according to the scanning strategy adopted.
- The point sources cannot be considered as one template in different frequencies, as each source has its own spectrum.
- The spectral index of the emissions due to dust and synchrotron has a spatial variation.
- The maps at different channels have different resolutions with beams not necessarily isotropic or spatially invariant.

This means to estimate the CMB, first the point sources should be detected and removed (or masked) at each individual channel, then different foreground emissions are removed and a CMB map is recovered using component separation techniques. The CMB power spectrum is then computed from the map, from which the cosmological parameters are estimated. A statistical analysis is also performed on the CMB map, which aims at, for e.g., determining the Gaussianity of the CMB or testing if it is isotropic as predicted in the theory. Other statistics such as measuring weak gravitational lensing or detecting weak gravitational waves are also part of the analysis.

In next sections, we describe in details these different steps, and we address the specific case of polarized data.

3 Point Sources

3.1 Matched Filter (MF)

This is defined as a linear filter that maximizes the amplification of the signal. Given a filter ψ (note that parts of the data that have similar shapes to the filter will be enhanced, therefore, the filter should have a similar shape to the sought signal) the filtered field is

$$w(x) = \int y(q)\psi(q)\mathrm{e}^{-iqx} dq \ , \tag{10}$$

where $y(q)$ is the Fourier transform of the data $y(x) = s(x) + n(x)$. It can be shown that the field will have the following shape at the position x_0 of the signal

$$w(x_0) = 2\pi \int qs(q)\psi(q)dq \ , \tag{11}$$

with variance

$$\sigma_w^2 = 2\pi \int qP(q)\psi^2(q)dq \ , \tag{12}$$

where $P(q)$ is the power spectrum of the noise: $\langle n(q)n^*(q')\rangle = P(q)\delta^2(q - q')$, with $n(q)$ being the Fourier transform of the noise $n(x)$. The point sources are recovered by satisfying two conditions: 1. $\langle w(x_0)\rangle = A$, where A is the amplitude of the signal at position x_0; 2. minimizing the variance σ_w^2 with respect to the filter ψ.

Applying this method to first year WMAP data [12] has produced a catalogue of 208 extragalactic point sources.

3.2 Mexican Hat Wavelet (MHW)

The Mexican Hat wavelet has been used for detection of point sources with Gaussian profiles [43]. The MHW is the second derivative of the Gaussian function, which has the following form in Fourier space

$$\psi(q) \propto \left(qR^2\right) \exp\left(-\frac{(qR)^2}{2}\right) \ , \tag{13}$$

where R is the scale of MHW. To detect the point sources the wavelet coefficient map at a given R is studied and those wavelet coefficients above a certain threshold are identified as point sources. The reason this works is that in the wavelet coefficient map a large fraction of the background is removed while the amplitude of the point sources are enhanced. Note that the enhancement depends on the scale R. Each image has an optimal scale that gives the maximum amplification for the point sources and this is determined from the data. The IFCA Mexican hat wavelet filter [66] is based on this method.

3.3 PowellSnake

PowellSnake [23] is a Bayesian approach. In this method the likelihood for the parameters characterizing the discrete objects is replaced by an alternative exact form, which makes it much quicker to evaluate. Rather than using MCMC methods to search the posterior to detect objects, the local maxima of the posterior are located in the parameter space that parametrizes the object. The maxima are located using a simultaneous multiple minimization code based on Powell's [76]. The method uses a 1-dimensional minimization algorithm, which in this case, is an enhanced version of the Brent's method[3]. The end-point of each minimization is a local maximum in the posterior, which gives the optimal parameters for the detected object. A Gaussian approximation to the posterior is then constructed about the peak and the detection is either accepted or rejected based on an evidence criterion; a Bayesian model selection is performed using an approximate evidence value based on a Gaussian approximation to the peak. This Gaussian approximation also provides the covariance matrix for the derived parameters of the objects. If the detection is accepted, then the detected object is subtracted from the map before the next minimization is launched.

3.4 SExtractor

One of the most widely used software packages for source detection is SExtractor [15]. Its success is in its ability to deal with very large images and its robustness. The first step in SExtractor is to estimate the background accurately to avoid any biases in the flux estimation. For this, the image is partitioned into blocks, and the local sky level in each block is estimated from its histogram [17, 49]. A filtering is applied to the background measurements in order to correct for spurious background values. Then, for an optimized detection, the image is convolved with a filter, the shape of which should match the shape of the sought signal. After, the pixels with values larger than a threshold level, T, are considered as significant, i.e. belonging to an object. The threshold level is generally chosen as $T = B + N\sigma$, where B is the background estimation at that pixel, σ is the standard deviation of the noise and N is a constant (typically $3-5$). The next step is to isolate the blended objects which are connected; sources which are extremely close to each other are deblended if a saddle point is found in the intensity distribution. Spurious detections due to neighboring bright objects are cleaned, and finally the centroids of each source is determined and a photometry in an elliptical Kron aperture [15, 57] is performed.

3.5 Sunyaev-Zeldovich (SZ) Cluster Extraction

The thermal SZ effect [94] is a spectral distortion of the CMB blackbody spectrum. This is caused by the inverse Compton scattering of the CMB photons by hot electrons in the interstellar gas of a galaxy cluster. There is also the kinetic SZ effect which is due to the radial peculiar velocities of clusters producing secondary anisotropies in the CMB via the Doppler effect. There are techniques

[3]Brent method is an interpolation scheme alternating between parabolic steps and golden sections.

for extraction of the kinetic SZ effect. However, as this emission is very weak its extraction is very challenging. Therefore, we focus on the extraction of the thermal SZ effect here.

The techniques for detection of the thermal SZ effect are very similar to the point source extraction techniques. This means the methods discussed above can easily be adapted to detect the SZ effect, by applying the correct profile of the sought signal. However, the thermal SZ effect has a very specific frequency signature that can be used to detect it — provided multifrequency observations are available. Such a multichannel matched filter was proposed in [69], and was selected by the Planck collaboration for the release of the Planck Early Sunyaev-Zeldovich Cluster Catalogue [74].

There are also other techniques that can be applied to a CMB map such as Biparametric Scale-Adapter Filter (BSAF) [67] and A Bayesian Approach [47]. Briefly, BSAF uses extra information apart from just the amplitude of the point sources. In particular it estimates the number of the maxima due to the background itself and compares it to the number of maxima due to the background plus the point sources by applying the Neyman-Pearson detector. The Bayesian approach is based on the evaluation of the posterior distribution $P(\theta|d)$ of the parameters θ given the data d. Two different strategies are proposed for the detection of compact sources: 1. an exact approach trying to detect all objects present in the data all at the same time; 2. an iterative approach (McClean algorithm). For both methods a Markov chain Monte Carlo technique is used to explore the parameters space modeling the objects.

For the Planck Early Release Compact Source Catalogue, PowellSnake and SExtractor were the two algorithms selected as they detected the largest number of sources with high reliability at high Galactic latitude; PowellSnakes for frequencies $30-143$GHz, and SExtractor for frequencies $217-857$GHz [74].

4 Component Separation

4.1 Modeling the sky emission

All components in a CMB sky observation are assumed to have emissions that can be separated into spatial and spectral parts so that an emission process j is written as

$$x_j(\nu,\, p) = a(\nu) s_j(p) \,, \tag{14}$$

and the observation has the form

$$y_i(p) = \sum_j x_j(\nu_i,\, p) + n_i(p) \,, \tag{15}$$

where i denotes the detector and $n_i(p)$ is the detector's noise contribution. For each component j this takes the form

$$\boldsymbol{y}(p) = \boldsymbol{A}\boldsymbol{s}(p) + \boldsymbol{n}(p) \,, \tag{16}$$

where $\boldsymbol{A}$ is the mixing matrix with the number of rows and columns representing the number of detectors and number of components respectively. The problem of component separation involves inverting the mixing matrix $\mathbf{A}$ giving a solution such that $\hat{\boldsymbol{s}} = \boldsymbol{W}\boldsymbol{y}$ is as good an estimator of $\boldsymbol{s}$ as possible. This is an ill posed problem dubbed the Blind Source Separation problem (BSS). Possible inversion methods include;

1. A simple inversion in the case of a square and non-singular $\boldsymbol{A}$; $\boldsymbol{W} = \boldsymbol{A}^{-1}$. The solution is unbiased, but may be noisy.
2. A pseudo-inverse in case of having more channels than components; $\boldsymbol{W} = \left[\boldsymbol{A}^{\dagger}\boldsymbol{A}\right]^{-1}\boldsymbol{A}^{\dagger}$. Here nothing is known about the level of noise and signal. Note that as there is no noise weighting one bad channel could contaminate all the data after inversion. The solution is unbiased.
3. A generalized least square solution in case of knowing the noise correlation matrix $\boldsymbol{C_n}$; $\boldsymbol{W} = \left[\boldsymbol{A}^{\dagger}\boldsymbol{C_n}^{-1}\boldsymbol{A}\right]^{-1}\boldsymbol{A}^{\dagger}\boldsymbol{C_n}^{-1}$. This is the best linear solution in the limits of high S/N. The solution is again unbiased.
4. A Wiener Solution in the case where the correlation between the sources, $\boldsymbol{C_s}$, is known; $\boldsymbol{W} = \left[\boldsymbol{A}^{\dagger}\boldsymbol{C_n}^{-1}\boldsymbol{A} + \boldsymbol{C_s}^{-1}\right]^{-1}\boldsymbol{A}^{\dagger}\boldsymbol{C_n}^{-1}$. One is minimizing the variance of a stochastic signal. This solution is biased, but can be debiased by multiplying the Wiener matrix by a diagonal matrix removing, for each mode, the impact of filtering. There is also a second form for the Wiener filter; $\boldsymbol{W} = \boldsymbol{C_s}\boldsymbol{A}^{\dagger}\left[\boldsymbol{C_n} + \boldsymbol{A}\boldsymbol{C_s}\boldsymbol{A}^{\dagger}\right]^{-1}$, where in the limits of high S/N it tends to the pseudo-inverse case.

The very first approach to derive the CMB is called 'template fitting' which, consists of fitting sky templates to all the non-CMB sky emissions and remove them from the maps. However, more advanced methods have been developed to tackle the BSS problem. For example, the Independent Component Analysis (ICA) methods have been developed which mostly rely on the statistical independence of the sources. Although independence is a strong assumption, it is in many cases physically acceptable, and provides much better solutions than using a simple second order decorrelation method, such as the Principal Component Analysis (PCA). Most of the ICA Methods, such as FastICA, assume that sources are statistically independent and non-Gaussian. However, there are also other ones, such as SMICA, which considers the case of mixed stationary Gaussian components and goes further by taking into account the additive instrumental noise. This method works in spherical harmonic domain, which has the advantage of better control of the beams of the instrument. Sparsity was also recently proposed for component separation and several methods have been extended to work in the wavelet domain, or to explicitly use a sparsity criterion. This section reviews a few methods for component separation.

4.2 Component Separation in the Pixel Domain

Template Fitting

Having the foregrounds as additional components of the microwave sky, one can perform a fit of the template to the data for foreground analysis. For template vector, T, the template-corrected data has the form

$$\tilde{\boldsymbol{y}} = \boldsymbol{y} - \sum_j \beta_j \boldsymbol{T}_j \ , \tag{17}$$

where the best-fit amplitude, β_j, for each foreground template can be obtained by minimizing $\tilde{\boldsymbol{y}}^T\boldsymbol{C}^{-1}\tilde{\boldsymbol{y}}$, where $\boldsymbol{C}$ is the total covariance matrix for the template-corrected data $\boldsymbol{C} = \left\langle \tilde{\boldsymbol{y}}\tilde{\boldsymbol{y}}^T \right\rangle$. The minimization leads to

$$\sum_j \boldsymbol{T}_j^T\boldsymbol{C}^{-1}\boldsymbol{T}_j\beta_j = \boldsymbol{T}_j^T\boldsymbol{C}^{-1}\boldsymbol{y} \ , \tag{18}$$

where $\boldsymbol{T}_j^T \boldsymbol{C}^{-1} \boldsymbol{T}_j$ has the information about the cross-correlation between the the templates themselves. This equation is equally valid in pixel space or harmonic space. However, in pixel space dealing with incomplete sky coverages is easier and, in addition, the noise is usually a diagonal matrix. On the other hand, in this space the signal covariance matrix is large and not sparse, where in harmonic space and under the assumption of Gaussianity, the signal covariance is diagonal. Although, approximating the noise as uniform and uncorrelated over the sky, one can make the noise covariance diagonal in this space too.

Template cleaning has a number of advantages, the first to be its simplicity. The technique makes full use of the spatial information in the template map, which is important for the non-stationary, highly non-Gaussian emission distribution, typical of Galactic foregrounds. It is also possible to fit multiple template maps to a single frequency channel, where in pixel-by-pixel techniques at least one frequency channel is required to fit each foreground component. There are also disadvantages to this technique and that is that imperfect models of the templates could add systematics and non-Gaussianities to the data. Refer to [28] for a more detailed description of template fitting techniques.

Template cleaning of the COBE/FIRAS data reduced a complicated foreground by a factor of 10 by using only 3 spatial templates [37]. WMAP team used a more complex technique, called the ILC, explained next, for their template fitting [39].

ILC: Internal Linear Combination

In this method very little is assumed about the different components in the signal. The main component is assumed to have the same template in all the frequency bands and the observations are calibrated with respect to this component. Data y has the form

$$y_i(p) = s(p) + f_i(p) + n_i(p) \, , \tag{19}$$

where i denotes the frequency channels, $f_i(p)$ and $n_i(p)$ are the foreground and noise contributions in pixel p respectively. One then looks for the solution

$$\hat{s}(p) = \sum_i w_i(p) y_i(p) \, , \tag{20}$$

where the weights $w_i(p)$ maximize a certain criterion about the reconstructed estimate $\hat{s}(p)$, while keeping the component of interest unchanged, and satisfy $\sum_i w_i = 1$. The simplest case is assuming the weights are independent of p and try to minimize the variance σ^2 of the estimated map. Hence having

$$\hat{s}(p) = s(p) + \sum_i w_i f_i(p) + \sum_i w_i n_i(p) \, , \tag{21}$$

under the assumption of decorrelation between $s(p)$ and all the foregrounds or noise. The variance of the ILC map is

$$\sigma^2 = \boldsymbol{w}^\dagger \boldsymbol{C} \boldsymbol{w} \, , \tag{22}$$

where $\mathbf{C} = \langle \mathbf{y}\mathbf{y}^\dagger \rangle$ with $\mathbf{y}$ and $\boldsymbol{w}$ standing for vectors of elements y_i and w_i. The minimum is obtained using the Lagrange multiplier method, which has as a solution

$$w_i = \frac{\sum_j \left[\boldsymbol{C}^{-1}\right]_{ij}}{\sum_{ij} \left[\boldsymbol{C}^{-1}\right]_{ij}} \, . \tag{23}$$

Note that the ILC method minimizes the *total* variance of the ILC map which means the weights are strongly constrained by regions close to the galactic plane where most of the foregrounds are constrained. Away from the galactic plane and on small scales, the best linear combination for cleaning the CMB map from foregrounds and noise might be different from regions close to the galactic plane or the large scales. To improve on this, the map is decomposed in several regions and ILC is applied to them independently. The ILC method is useful when no prior information is known about the different components (in this method the only prior knowledge is the CMB behavior). Therefore, it is more of a foreground removal than a component separation technique. Prior information about the different astrophysical components, if present, can be used in efficiently removing their contributions to the CMB sky. In particular their morphology, their localization, their frequency scaling can be used in understanding their emission in the CMB sky.

FastICA

FastICA [48] solves a Blind Source Separation (BSS)[4] problem. The simplest mixture model takes the form $\boldsymbol{y} = \boldsymbol{A}\boldsymbol{s}$ where as before $\boldsymbol{A}$ is the mixing matrix and the entries of $\boldsymbol{s}$ are assumed to be independent random variables. Note that the independent sources can only be recovered up to a permutation and a scaling of the entries of $\boldsymbol{s}$. Although independence is a strong assumption, it is in many cases physically plausible.

Independent Component Analysis (ICA) methods were developed to solve the BSS problem. Algorithms for BSS and mixing matrix estimation depend on the model used for the probability distribution of the sources. In a first set of techniques, source separation is achieved in a noise-less setting, based on the non-Gaussianity of all but possibly one of the components. Most mainstream ICA techniques belong to this category, e.g. FastICA. In a second set of blind techniques, the components are modeled as Gaussian processes, either stationary or non-stationary and, in a given representation, separation requires that the sources have non-proportional variance profiles. Moving to a Fourier representation, the idea is that colored components can be separated based on the diversity of their power spectra.

The FastICA technique is meant for the analysis of a combination of independent non-Gaussian sources in a noise-less setting. It is a so-called orthogonal ICA method where the components are sought by maximizing a measure of non-Gaussianity assuming they are independent. Non-Gaussianity is assessed in FastICA using a contrast function G based on a non-linear approximation to neg-entropy [48]. In a simple deflation scheme (for spherical data) the directions are found sequentially: a direction r of maximal non-Gaussianity is sought by maximizing

$$J_G(r) = \left(\mathcal{E}\{G(r^T y_{\text{white}})\} - \mathcal{E}\{G(\mu)\}\right)^2 , \tag{24}$$

where $\mathcal{E}$ is the expectation operator, y_{white} is the renormalized data and μ stands for centered unit variance Gaussian variable, under the constraint that r has unit norm and is orthogonal to the directions found previously. For example, the contrast function G can be $G_0(u) = (1/a)\log(\cosh(au))$, where a is a constant to be determined depending on the application [48]. A complete description of this method can be found in [48] and references therein.

[4]BSS is a problem that occurs in multi-dimensional data processing where the overall goal is to recover unobserved sources $\boldsymbol{s}$ from a mixture of them $\boldsymbol{y}$, without assuming any forms for the sources.

Correlated Component Analysis (CCA)

This method [9] is a semi-blind approach that estimates the mixing matrix on sub-patches of the sky based on second order statistics of the data. It makes no assumptions about the independence of the sources. This method adopts the commonly used models for the sources to reduce the number of parameters estimated and exploits the spatial structure of the source maps. The spatial structure of the maps are accounted for through the covariance matrices at different shifts (τ, ψ)

$$\boldsymbol{C}_d(\tau, \psi) \quad = \quad \boldsymbol{A}\boldsymbol{C}_s(\tau, \psi)\boldsymbol{A}^t + \boldsymbol{C}_n(\tau, \psi) \ , \tag{25}$$

where $\boldsymbol{C}_d(\tau, \psi)$ is estimated from data and the noise covariance matrix $\boldsymbol{C}_n(\tau, \psi)$ is derived from the map-making noise estimations. Then by minimizing the equation

$$\sum_{\tau,\psi} \left\| \boldsymbol{A}\boldsymbol{C}_s(\tau, \psi)\boldsymbol{A}^t - [\boldsymbol{C}_d(\tau, \psi) - \boldsymbol{C}_n(\tau, \psi)] \right\| \ , \tag{26}$$

where the Frobenius norm is used, one can estimate the mixing matrix and the free parameters of the source covariance matrix. Given as estimate of $\boldsymbol{C}_s$ and $\boldsymbol{C}_n$, the above equation can be inverted and component maps obtained via the standard inversion techniques of Wiener filtering or generalized least square inversion. To obtain a continuous distribution of the free parameters of the mixing matrix, CCA is applied to a large number of partially overlapping patches.

4.3 Component Separation in the Spherical Harmonic Domain

Maximum Entropy Method (MEM)

Having a hypothesis H in which the measured data d is a function of the underlying signal s one can follow Bayes' theorem, which tells us the posterior probability is the product of the likelihood and the prior probability divided by the evidence;

$$P(s|d, H) = \frac{P(d|s, H)P(s|H)}{P(d|H)} \ . \tag{27}$$

Then following the maximum entropy principle, one uses a prior distribution which maximizes the entropy given a set of constraints. Hobson and collaborators [46] argue that for such purposes an appropriate prior for the astrophysical components $\boldsymbol{s}$ is

$$P(\boldsymbol{s}) = \exp\left[-\alpha S_c(\boldsymbol{s}, \, \boldsymbol{m}_u, \, \boldsymbol{m}_v)\right] \ , \tag{28}$$

$$S_c = \sum_j \left\{ \left[s_j^2 + 4m_{uj}m_{vj}\right]^{1/2} - m_{uj} - m_{vj} - s_j \ln\left[\frac{\left[s_j^2 + 4m_{uj}m_{vj}\right]^{1/2} + s_j}{2m_{uj}}\right] \right\} \ , \tag{29}$$

where $\mathbf{m_u}$ and $\mathbf{m_v}$ represent the astrophysical components. The MEM can be implemented in the spherical harmonic domain where the separation is performed mode-by-mode which speeds up the optimization. FastMEM is an algorithm based on this; it is a non-blind method, which means the spectral behavior of the components must be known beforehand. Further details of this method are presented in [91].

Spectral Matching ICA (SMICA)

This technique also solves a BSS problem, but is computationally very different from FastICA. SMICA [27] is based on spectral statistics that are localized in frequency instead of space, which are simply the spectra of the channels. For multichannel maps $y_i(p)$ one computes

$$\hat{\boldsymbol{R}}_\ell = \frac{1}{2\ell+1} \sum_m \boldsymbol{y}_{\ell m} \boldsymbol{y}_{\ell m}^\dagger \, , \tag{30}$$

for each ℓ and m. One then models the ensemble-average as $\boldsymbol{R}_\ell = \left\langle \hat{\boldsymbol{R}}_\ell \right\rangle = \sum_j \boldsymbol{R}_\ell^j$ where the sum is over the components. For each component, $\boldsymbol{R}_\ell^j$ is a function of a parameter vector θ^j, where the parameterization embodies the prior knowledge about the components. The parameters are determined by minimizing the *spectral mismatch*

$$\min_\theta \sum_\ell (2\ell+1) K(\hat{\boldsymbol{R}}_\ell | \sum_j \boldsymbol{R}_\ell^j) \, , \tag{31}$$

where $K(\boldsymbol{C}_1|\boldsymbol{C}_2)$ is a measure of mismatch between $\boldsymbol{C}_1$ and $\boldsymbol{C}_2$.

4.4 Component Separation in the Wavelet Domain

Toward Wavelet Based Methods

Working in the pixel space has the advantage of decomposing the sky into patches and processing them independently. Having a mixing matrix per patch, one can have a better grasp of the spatial variation of the total matrix. The smaller the patches are the better the variations are captured, but the higher the noise is, so there is a trade off between the two. Working in the spherical harmonic domain makes the spatial variation analysis harder but has the advantage of better modeling of the beam.

Working in the wavelet space is a way to use the best of both worlds. By making use of undecimated wavelet transform, one can transform each channel into the wavelet domain, partition each wavelet band into blocks and perform a component separation per frequency band, per patch. Wavelets tend to grab the informative coherence between pixels while averaging the noise contributions, thus enhancing structures in the data. Hence a wavelet representation often leads to a more robust noise. Following this principle, ILC and SMICA have been extended to use wavelets [35], [71].

Generalized Morphological Component Analysis (GMCA)

This method again solves a BSS problem, but goes further by using the sparsity of the components in the wavelet domain [18].

Assume $\boldsymbol{\Phi}$ is a signal representation (such as wavelet basis, curvelet frame, etc.) in which each source is assumed to be sparse; $s_j = \boldsymbol{\Phi}\alpha_j$, where α_j are the decomposition coefficients. The sparsity of the sources means that most of the entries of α_j are equal or very close to zero. The multichannel noiseless data $\boldsymbol{y}$ can be written as

$$\boldsymbol{y} = \boldsymbol{A}\alpha\boldsymbol{\Phi}^T \, , \tag{32}$$

where the GMCA seeks an unmixing scheme through the estimation of $\boldsymbol{A}$, which leads to the sparsest sources $\boldsymbol{s}$. This is expressed by the following optimization problem written in the augmented Lagrangian form

$$\min \frac{1}{2} \|\boldsymbol{y} - \boldsymbol{A}\alpha\boldsymbol{\Phi}\|_F^2 + \lambda \sum_j \|\alpha_j\|_p \ , \tag{33}$$

where typically $p = 0$ (or its relaxed convex version with $p = 1$) and $\|\boldsymbol{X}\|_{\mathrm{F}} = \left(\mathrm{trace}(\boldsymbol{X}^T\boldsymbol{X})\right)^{1/2}$ is the Frobenius norm. The details of this method is presented in [18], where it is shown that the GMCA is very robust to noise.

4.5 Comments

As presented above, there are many methods proposed to tackle the difficulties of component separation. They all work differently and depending on what the final scientific goal is one might perform better than the others. For example, one may work better on large scales while another could do a better job on small scales. Therefore, the "best" map could be different depending on what the goal is. A first comparison of methods has been done in [60]. Also, with the future Planck release in early 2014, we will certainly have a much better understanding of what methods work better to recover the CMB map for Planck.

5 Power Spectrum Estimation

As discussed before, if the statistical properties of the CMB fluctuations are isotropic and Gaussian all the cosmological information in a sky map is contained in its power spectrum. This means that all the information from a data set can be reduced to just a few thousand numbers, greatly facilitating parameter estimation. However, a straightforward expansion in spherical harmonics is not the best way to measure the power spectrum: 1. one always has incomplete sky coverage; 2. one wishes to give less weight to noisier pixels in order not to destroy information. Both of these facts spoil the orthogonality of the spherical harmonics. Any quadratic combination of pixels will, when appropriately normalized, measure some weighted average of the power spectrum - the weights are known as the window function. The non-orthogonality simply means that it is impossible to obtain an ideal (Kronecker delta) window function. Instead, the best you can do is to get a window function whose width is about the inverse of the smallest angular map dimension in radians, which is usually adequate for all practical purposes adequate.

To be able to use the power spectrum for estimation of the cosmological parameters, one needs to know the complete likelihood function $P\left(d|C_\ell(\boldsymbol{\theta})\right)$, where $\boldsymbol{\theta}$ are the underlying cosmological parameters. Hence an important output of the power spectrum estimation step is a prescription for evaluation of the model spectra likelihood function. However, this evaluation is not computationally feasible at the full map resolution and hence there are different methods to calculate the likelihood function at low and high ℓ. The low-ℓ codes use low resolution maps (eg. Healpix maps of $N_{side} =$ 8, 16) and determine the properties of the likelihood as a function of the C_ℓ parameters using Bayesian statistics. The high-ℓ codes use unbiased frequentist estimators to form quadratic functions of the data (pixels of the map) and determine $\widehat{C}_\ell$, such that $\left\langle \widehat{C}_\ell \right\rangle = C_\ell$. Below we will summarize a few codes.

5.1 Low-ℓ Codes

MADCAP

MADCAP maximizes the log-likelihood function using a quasi Newton-Raphson (NR). It uses the Fisher matrix

$$F_{\ell\ell'} = \frac{1}{2}\mathrm{trace}\left(\boldsymbol{C}^{-1}\frac{\partial \boldsymbol{C}}{\partial C_\ell}\boldsymbol{C}^{-1}\frac{\partial \boldsymbol{C}}{\partial C_{\ell'}}\right) , \tag{34}$$

to find the location where

$$\frac{\partial \ln P(\boldsymbol{d}|C_{\ell'})}{\partial C_\ell} = 0 . \tag{35}$$

The NR iteration step involves

$$\delta C_\ell = \frac{1}{2}\sum_{\ell'}(F^{-1})_{\ell\ell'}\left[\boldsymbol{d}^t\boldsymbol{C}^{-1}\frac{\partial \boldsymbol{C}}{\partial C_\ell}\boldsymbol{C}^{-1}\boldsymbol{d} - \mathrm{trace}\left(\boldsymbol{C}^{-1}\frac{\partial \boldsymbol{C}}{\partial C_{\ell'}}\right)\right] . \tag{36}$$

In some cases it is necessary to bin the C_ℓ to make the calculations computationally feasible. The binned power spectrum satisfies $C_\ell = \sum_{\ell \in b} C_b P_\ell$, where P_ℓ is the shape function usually taking the form $P_\ell \propto (\ell(\ell+1))^{-1}$.

BolPol is a similar quadratic maximum likelihood (QML) estimator, which is equivalent to one step of NR iteration. Presently, it can handle maps of Healpix resolution $N_{side} = 32$. BoLike is another similar code which can provide likelihood based confidence intervals. Refer to [41] where both of these methods have been applied to WMAP data.

Commander (Gibbs Sampling)

The Commander [33] algorithm maps out the joint CMB-foreground posterior distribution by sampling. This method is a very general and flexible, which means any parametric foreground model can be included in the analysis. It provides the exact joint CMB and foreground posterior distributions, from which the exact marginal CMB power spectrum and sky signal posterior distributions can be obtained.

The idea behind this technique is to draw samples from the joint density $P(C_\ell, \boldsymbol{s}|\boldsymbol{d})$ and then marginalize over the signal to obtain probability density $P(C_\ell|\boldsymbol{d})$. This is because the theory of Gibbs sampling states that sampling from the conditional densities $P(\boldsymbol{s}|C_\ell, \boldsymbol{d})$ and $P(C_\ell|\boldsymbol{s}, \boldsymbol{d})$ will converge to sampling from the joint density $P(C_\ell, \boldsymbol{s}|\boldsymbol{d})$ after the initial burn-in period. As the joint distribution is probed one can quantify joint uncertainties if desired. The map sampling process is performed in solving the following two equations simultaneously. The first is to solve for the mean field map $\boldsymbol{x}$

$$\left[\boldsymbol{C}^{-1} + \left(\sum_i \boldsymbol{A}_i^T\boldsymbol{C}_{n,i}^{-1}\boldsymbol{A}_i\right)\right]\boldsymbol{x} = \sum_i \boldsymbol{A}_i^T\boldsymbol{C}_{n,i}^{-1}\boldsymbol{d}_i , \tag{37}$$

$$\left[\boldsymbol{C}^{-1} + \left(\sum_i \boldsymbol{A}_i^T\boldsymbol{C}_{n,i}^{-1}\boldsymbol{A}_i\right)\right]\boldsymbol{y} = \boldsymbol{C}^{-1/2}\omega^0 + \sum_i \boldsymbol{A}_i^T\boldsymbol{C}_{n,i}^{-1/2}\omega_i , \tag{38}$$

where $\boldsymbol{d}_i$ is the residual signal map i and ω_i are Gaussian white noise maps having zero mean and unit variance. Any other component one may wish to include in the analysis will be subtracted from the data so that an actual residual map can be formed, from which the mean field map is computed.

The mean field map is a generalized Wiener filtered map, meaning it is biased. For constructing an unbiased sample one must add a fluctuation map having the properties such that the sum of the two fields forms a sample from the distribution of the correct mean and covariance. The second equation above is the appropriate equation for this fluctuation map.

TEASING is another method that approximates the low-ℓ likelihood using; 1. parametric models for the conditional and marginal likelihood; 2. a Gaussian copula model to assemble the marginal distribution into a joint distribution. For further information about TEASING refer to [10].

5.2 High-ℓ Codes

MASTER

Monte Carlo Apodized Spherical Transform Estimator (MASTER) [45] is a method based on a direct spherical harmonic transform (SHT) of the CMB map and allows one to implement particular properties of a given CMB experiment, such as the survey geometry, instrumental noise behavior, etc.. The unwanted contribution of the instrumental noise, any necessary alteration of either the recorded data stream or the raw map of the sky (introduced during the data analysis) can be calibrated in Monte Carlo (MC) simulations of the modeled observation and can then be removed or corrected for in the estimated power spectrum. The harmonic mode-mode coupling, which is induced by the incomplete sky coverage, can analytically be corrected for to obtain an unbiased estimated power spectrum.

One can define a pseudo-power spectrum $\tilde{C}_\ell$ as

$$\tilde{C}_\ell = \frac{1}{2\ell+1} \sum_{m=-\ell}^{\ell} |\tilde{a}_{\ell m}| \ , \tag{39}$$

where $2\ell + 1$ are the number of degrees of freedom and the coefficients $\tilde{a}_{\ell m}$ are defined as

$$\begin{aligned} \tilde{a}_{\ell m} &= \int d\Omega \Theta(\Omega) W(\Omega) Y^*_{\ell m} && (40) \\ &\approx \Omega_p \sum_p \Theta(p) W(p) Y^*_{\ell m}(p) \ . && (41) \end{aligned}$$

$W(\Omega)$ is a position-dependent weighting function applied to the map. The integral over the whole sky is approximated by a summation over the pixels (with surface area Ω_p) of the CMB map. The ensemble average of this spectrum is related to the full-sky angular spectrum C_ℓ by

$$\left\langle \tilde{C}_\ell \right\rangle = \sum_{\ell'} M_{\ell\ell'} F_{\ell'} B^2_{\ell'} \left\langle C_{\ell'} \right\rangle + \left\langle \tilde{N}_\ell \right\rangle \ , \tag{42}$$

where $M_{\ell\ell'}$ describes the effect of mode-mode coupling due to the cut sky, B_ℓ is a window function taking care of the smoothing effects of the beam and finite pixel size, F_ℓ is a transfer function modeling the filtering that is applied to the data/maps and $\left\langle \tilde{N}_\ell \right\rangle$ is the average power spectrum of the noise, which can be extracted from the actual data stream.

To reduce the correlations between the C_ℓ, which is induced by the cut sky, and also to reduce the errors on the estimated power spectrum, one can bin the power spectrum in ℓ. The binned power spectrum is $\mathcal{C}_b = P_{b\ell} C_\ell$, where P is the binning operator. Therefore, an unbiased estimator for the power spectrum of the whole sky is given by

$$\hat{\mathcal{C}}_b = K^{-1}_{bb'} P_{b'\ell} \left(\tilde{C}_\ell - \left\langle \tilde{N}_\ell \right\rangle_{\text{Monte Carlo}} \right) \,, \tag{43}$$

where $K_{bb'} = P_{b\ell} M_{\ell\ell'} F_{\ell'} B^2_{\ell'} Q_{\ell' b}$ and $Q_{\ell b} P_{b\ell'} \langle C_{\ell'} \rangle = Q_{\ell b} \langle \mathcal{C}_b \rangle$, with an estimator of the noise having the form

$$\hat{\mathcal{N}}_b = K^{-1}_{bb'} P_{b'\ell} \left\langle \tilde{N}_\ell \right\rangle_{\text{Monte Carlo}} \,. \tag{44}$$

This methods has been successfully applied to the WMAP map; in this case a hybrid method was used for the power spectrum estimation, where for $\ell \leq 32$ the spectrum is obtained using a Blackwell-Rao estimator applied to a chain of Gibbs samples and for $\ell > 32$ the spectrum is derived from the MASTER pseudo-C_ℓ quadratic estimator [11].

cROMAster is an implementation of the MASTER method extended to polarization [56] and has been applied to BOOMERang data [70, 52]. CrossSpect is again a pseudo-C_ℓ [45] estimator that computes cross power spectra from two different detectors. XFaster [80] is again a similar method based on MASTER to estimate the pseudo-C_ℓ for temperature and polarization.

Xpol

Xpol estimates the angular power spectra by computing the cross-power spectra between different input maps of multiple detectors of the same experiment or from different instruments, calculating analytical error bars for each of the maps. The cross-power spectra are then combined by making use of a Gaussian approximation for the likelihood function. The method also computes an analytical estimate of the cross-correlation matrix from the data, avoiding any Monte Carlo simulations.

For each power spectra, Xpol can estimate the cross-correlation matrix at different multipoles, from which error bars and the covariance matrix can be deduced for each cross-power spectra. In the limit of large sky coverage [31], one obtains [96]:

$$\Xi^{XY,X'Y'}_{\ell\ell'} = \mathcal{M}^{-1}_{\ell\ell_1}(XY) \left[\frac{\mathcal{M}^{(2)}_{\ell_1\ell_2}(XX',YY') C^{XX'}_{\ell_1} C^{YY'}_{\ell_2}}{2\ell_2+1} + \frac{\mathcal{M}^{(2)}_{\ell_1\ell_2}(XY',X'Y) C^{XY'}_{\ell_1} C^{X'Y}_{\ell_2}}{2\ell_2+1} \right] \left(\mathcal{M}^{-1}_{\ell'\ell_2}(X'Y') \right)^t , \tag{45}$$

with

$$\mathcal{M}_{\ell\ell'}(XY) = E^X_\ell E^Y_\ell M_{\ell\ell'}(XY) \,,$$
$$\mathcal{M}^{(2)}_{\ell\ell'}(XX',YY') = E^X_\ell E^{X'}_\ell M^{(2)}_{\ell\ell'}(XX',YY') E^Y_{\ell'} E^{Y'}_{\ell'} \,,$$

where $X, Y \in \{T, B, E\}$; $M_{\ell\ell'}(XY)$ is the coupling kernel matrix analytically determined from sky masks for X and Y; $M^{(2)}$ is the quadratic coupling matrix determined from the mask product for X and X'correlated with the mask product for Y and Y'; $E_\ell = p_\ell B_\ell \sqrt{F_\ell}$, where p_ℓ is the transfer function describing the smoothing effect induced by the finite pixel size.

To obtain the best estimate of the power spectrum $\tilde{C}_\ell$ by combining the cross power spectra, one needs to maximize the Gaussian approximated likelihood function

$$-2 \ln \mathcal{L} = \sum_{XY,X'Y'} \left[\left(C^{XY}_\ell - \tilde{C}_\ell \right) |\Xi^{-1}|^{XY,X'Y'}_{\ell\ell'} \left(C^{X'Y'}_{\ell'} - \tilde{C}_{\ell'} \right) \right] \,, \tag{46}$$

and the estimate of the angular power spectrum is (ignoring correlation between adjacent multipoles)

$$\tilde{C}_\ell = \frac{1}{2} \frac{\sum_{XY,X'Y'} \left[|\Xi^{-1}|_{\ell\ell}^{XY,X'Y'} C_\ell^{X'Y'} + C_\ell^{XY} |\Xi^{-1}|_{\ell\ell}^{XY,X'Y'} \right]}{\sum_{XY,X'Y'} |\Xi^{-1}|_{\ell\ell}^{XY,X'Y'}} . \tag{47}$$

This method has been used on Archeops data to estimate the CMB angular power spectrum [96] and the polarized foreground emission at the sub-millimeter and millimeter wavelength in [75].

SPICE

This method differers from the previous methods by introducing the angular correlation function of the signal at distance θ

$$\xi(\theta) = \sum_\ell \frac{2\ell+1}{4\pi} C_\ell P_\ell(\theta) , \tag{48}$$

where $P_\ell(\theta)$ is the Legendre Polynomial. The ensemble average of the measured correlation function satisfies $\left\langle \tilde{\xi}(\theta) \right\rangle = \xi^W(\theta)\xi(\theta) + \xi^N(\theta)$, where $\xi^W(\theta)$ and $\xi^N(\theta)$ are the weighting and noise correlation functions respectively [95]. The advantage of this method over MASTER is that the matrix inversion in the MASTER method (Eq. 42) becomes a division by ξ^W. The full sky C_ℓ is then given by

$$C_\ell \equiv 2\pi \sum_i w_i \xi(\theta_i) P_\ell(\theta_i) , \tag{49}$$

where w_i are the weights of the Gauss-Legendre quadrature.

6 Cosmological Parameters

Once computed from the data, the power spectrum can be used to constrain cosmological models. The power spectrum is a complicated-looking function, because it depends on virtually all cosmological parameters. Therefore we can use an observed power spectrum to measure the cosmological parameters.

A parameter estimation with a simple χ^2 model fit to the observed power spectrum will give virtually the smallest error bars possible. There are several methods for estimating the cosmological parameters. Here we present the most popular method, Markov Chain Monte Carlo (MCMC) simulations. In this method the idea is to generate a random walk through the parameter space which then converges towards the most likely parameter values. This is an iterative process. At each step a sample of parameters is chosen (Monte Carlo) from a proposal probability density. The likelihood for that sample is calculated and depending on the criterion (that only depends on the previous likelihood function value) the likelihood is accepted or rejected (Markov Chain). This is called the Metropolis-Hastings algorithm. The code CosmoMC [62] is based on this procedure. Below, we will go through the necessary steps involved in a MCMC run for the cosmological parameter estimation.

As explained above, MCMC is a random walk in the parameter space where the probability of picking a set of parameters at any step is proportional to the posterior distribution $P(\boldsymbol{\theta}|d)$:

$$P(\boldsymbol{\theta}|d) = \frac{P(d|\boldsymbol{\theta})P(\boldsymbol{\theta})}{\int P(d|\boldsymbol{\theta})P(\boldsymbol{\theta})d\boldsymbol{\theta}} , \tag{50}$$

where $P(d|\boldsymbol{\theta})$ is the likelihood of the data d given the parameters $\boldsymbol{\theta}$ and $P(\boldsymbol{\theta})$ holds the prior knowledge about the parameters. Here is the necessary steps for each chain:

1. Start with an initial set of cosmological parameters $\boldsymbol{\theta}_1$ to compute the C_ℓ^1 and the likelihood $P_1 = P(d|\boldsymbol{\theta_1}) = P(\hat{C}_\ell|C_\ell^1)$.

2. Take a random step in the parameter space obtaining a new set of parameters $\boldsymbol{\theta}_2$. Compute the C_ℓ^2 and the likelihood P_2 for this new set.

3. If $P_2/P_1 > 1$, save $\boldsymbol{\theta}_2$ as the new set of cosmological parameters and repeat step 2.

4. If $P_2/P_1 < 1$, draw a random number x from a uniform distribution from 0 and 1. If $x > P_2/P_1$, save $\boldsymbol{\theta}_1$ and return to step 2. If $x < P_2/P_1$ save $\boldsymbol{\theta}_2$ as the parameters set, i.e. do as in 4.

5. Stop the chains when the convergence criterion is satisfied and the chains have enough points for a reasonable presentation of the posterior distributions.

Here we present an example of a convergence criterion that was used for WMAP first year data analysis. Assume having M chains, each having $2N$ elements, of which only N is used. Therefore, y_i^j denotes a point in the parameter space with $i = 1, ..., N$ and $j = 1, ..., M$. The following expressions can be defined:

mean of the chains

$$\bar{y}^j = \frac{1}{N} \sum_i y_i^j \ ,$$

mean of the distribution

$$\bar{y} = \frac{1}{NM} \sum_{ij} y_i^j \ ,$$

variance between chains

$$B_n = \frac{1}{M-1} \sum_j \left(\bar{y}^j - \bar{y}\right)^2 \ ,$$

and variance within a chain

$$W = \frac{1}{M\,(N-1)} \sum_{ij} \left(y_i^j - \bar{y}^j\right)^2 \ .$$

Then the quantity

$$\hat{R} = \frac{\frac{N-1}{N} W + B_n \left(1 + \frac{1}{M}\right)}{W} \ ,$$

monitors the convergence by requiring $\hat{R} < 1$ for converged chains. A few other codes for cosmological parameter estimation include, for e.g., PICO [36], CosmoPMC [54], CosmoNet [6]. Further details on MCMC and cosmological parameter estimation can be found in [97, 81, 64, 98, 42].

7 CMB Map Statistical Analysis

The CMB observations so far have confirmed a standard model of the Universe predicting that the primordial fluctuations are a 'realization' of a Gaussian random field. This means that the CMB fluctuations can be completely described by a power spectrum. However, there are several inflationary models that predict departures from Gaussianity that are detectable with the current CMB experiments. To measure the amount of non-Gaussianity, the CMB bispectrum (the three point correlation function in harmonic space) is measured.

Indeed, the non-Gaussian signatures in the CMB can be related to very fundamental questions such as the global topology of the Universe [79], topological defects such as cosmic strings [19], and multi-field inflation [13], etc.. However, the non-Gaussian signatures can also have non-cosmological origins; the SZ effect [93], gravitational lensing by large scale structures [14] or the reionization of the Universe [5, 24]. They may also be due to foreground emission [50] or to non-Gaussian instrumental noise and systematics [8]. All these sources of non-Gaussian signatures might have different origins and thus different statistical and morphological characteristics. Many approaches have been investigated to detect the non-Gaussian signatures: Minkowski functionals and the morphological statistics [84], the bispectrum and trispectrum [65, 58], wavelet and curvelet transforms [5, 38, 25, 87]. Describing all these methods are outside the scope of this chapter.

As the component separation cannot be perfect, some level of residual contributions, most significantly in the galactic region and at the locations of strong radio point sources will unavoidably contaminate the estimated spherical CMB maps. Therefore, it is common practice to mask out those parts of the data (*e.g.* using the mask shown on Figure 3, provided by the WMAP team) in order for instance to reliably assess the non-Gaussianity of the CMB field through estimated higher order statistics (e.g., skewness, kurtosis) in various representations (e.g., wavelet, curvelet, etc.) [51] or to estimate the bispectrum of the CMB spatial fluctuations. But the gaps in the data thus created need to be handled properly. For most previously mentioned methods, masked data is a nightmare. Indeed, the effect of the mask on a given statistic may be much larger than the weak signal we are trying to detect.

Sparse Inpainting as a Solution to the Curse of Missing Data

In order to restore the *stationarity* of a partly incomplete CMB map and thus lower the impact of the missing data on the estimated measures of non-Gaussianity or on any other non-local statistical test, it was proposed to use an inpainting algorithm on the sphere to fill in and interpolate across the masked regions. The grounds of the inpainting scheme are in the notion of the sparsity of the data set as discussed in the component separation section.

The inpainting problem can be set out as follows: Let X be the ideal complete image, Y be the observed incomplete image and $\mathcal{M}$ be the binary mask (i.e. $\mathcal{M}_i = 1$ if pixel i has information and $\mathcal{M}_i = 0$ otherwise), hence having $Y = \mathcal{M}X$. Inpainting then aims to recover X, knowing Y and $\mathcal{M}$. Therefore, one aims to minimize

$$\min_X \|\mathcal{S}X\|_0 \quad \text{subject to} \quad Y = \mathcal{M}X \ , \tag{51}$$

where $\mathcal{S}$ is the spherical harmonic transform. It was shown in [32] that this optimization problem can efficiently be solved through an iterative thresholding algorithm called MCA:

$$X^{n+1} = \Delta_{\mathcal{S}}^{\lambda_n}(X^n + Y - \mathcal{M}X^n) \ , \tag{52}$$

where the nonlinear operator $\Delta_{\mathcal{S}}^{\lambda}(Z)$ 1. decomposes the signal Z onto the spherical harmonics giving the coefficients $\alpha = \mathcal{S}Z$, 2. performs hard/soft thresholding on the coefficients and, 3. reconstructs $\tilde{Z}$ from the thresholded coefficients $\tilde{\alpha}$. In the iteration the threshold parameter λ_n decreases with the iteration number working similarly to the cooling parameter of the simulated annealing techniques, i.e. it allows the solution to escape from local minima. More details on optimization in inpainting with sparsity can be found in [89] and the theories behind inpainting on a sphere can be found in [77].

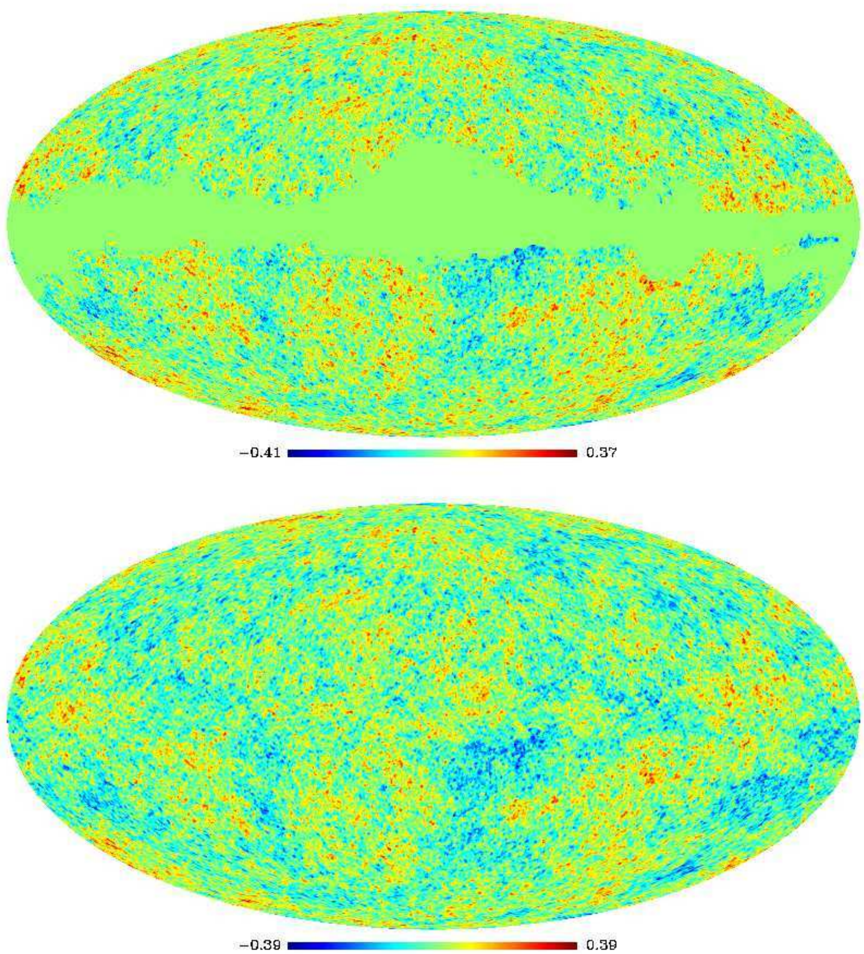

Figure 3: Top: CMB data map provided by the WMAP team. Areas of significant foreground contamination in the galactic region and at the locations of strong radio point sources have been masked out. Bottom: Map obtained by applying the MCA-inpainting algorithm on the sphere to the former incomplete WMAP CMB data map.

A simple numerical experiment is shown in Fig. 3, starting with the full-sky CMB map provided by the WMAP team. This CMB map was partially masked at the pixels where the level of contamination by residual foregrounds is high. Applying the inpainting algorithm, making use of the sparsity of the representation of CMB in the spherical harmonics domain, leads to the map shown on the right of Fig. 3: the stationarity of the CMB field appears to have been restored. It was shown in [2, 3] that inpainting the CMB map is an interesting approach for analyzing it, especially for non-Gaussianity studies and power spectrum estimation.

The sparse inpainting technique has been used in reconstruction of the CMB lensing [73] and measuring the ISW effect [30].

8 Polarization

One of the main goals of the Planck experiment is to constrain the polarization of CMB to a scale never done before. This is of great importance as the data will help break several degeneracies that currently exist. The CMB polarization will also help probe the reionization era as the large scale polarization, on scales of tens of degrees ($\ell > 10$), is generated at the time reionization. The analysis of the CMB polarization data are very similar to the temperature data. However, some new complications exist in their analysis due to the tensorial nature of the polarization field. In addition the small amplitude of the CMB polarization means a more careful control of the systematics is necessary[5]. This also makes the polarization data analysis more instrument specific. In spite of the extra complications, the steps presented in the temperature pipeline above can easily be applied to the case of polarization by a simple generalization. A generalization means that the TOD for the polarization data can be written as

$$\begin{aligned} d_t &= s_t + n_t & (53)\\ &= A_{tp} s_p + n_t & (54)\\ &= A_{tp}\left(I_p + Q_p \cos 2\psi_t + U_p \sin 2\psi_t\right) + n_t \ , & (55) \end{aligned}$$

where A_{tp}, n_t are the pointing matrix and the noise respectively, ψ_t is the angle between the direction of the detector at time t and the ϕ-direction on the sky. The Stokes parameter I, U and Q measure the total intensity (I) and the linear polarization (Q and U). For full sky analysis they are decomposed into spin ± 2 spherical harmonics as

$$Q(\hat{\boldsymbol{n}}) \pm iU(\hat{\boldsymbol{n}}) = \sum_{\ell m} a_{\pm 2,\ell m\, \mp 2} Y_{(\ell m)}(\hat{\boldsymbol{n}}) \ . \tag{56}$$

The spin ± 2 spherical harmonic coefficients, $a_{\pm 2,\ell m}$, are then decomposed into E and B modes as

$$a_{\pm 2,\ell m} = -\left(a^E_{\ell m} \pm i a^B_{\ell m}\right) \ , \tag{57}$$

with $a^E_{\ell m} = (-1)^m a^{E*}_{\ell - m'}$ and $a^B_{\ell m} = (-1)^m a^{B*}_{\ell - m'}$. This decomposition introduces an extra step in the pipeline presented above, which is the $E - B$-mode separation in the map-making step. The separation can also be done in the power spectrum step, however, a map-level separation is very useful as, for e.g., analyzing the B-mode would be a useful diagnostic of foreground residuals or unknown systematic effects. The separation amounts to solving for the potentials P_E and P_B in the rank-2 symmetric trace-free tensor, $\mathcal{P}_{ab}$,

$$\mathcal{P}_{ab} = \nabla_{\langle a} \nabla_{b\rangle} P_E + \epsilon^c_{\langle a} \nabla_{b\rangle} \nabla_c P_B \ , \tag{58}$$

where angle brackets denote the trace-free, symmetric part of the indices, ∇_a is the covariant derivative on the sphere and ϵ_{ab} is the alternating tensor. Note that the maps of the Q and U polarization

[5]The CMB radiation has a partial linear polarization with r.m.s of $\sim 6\mu$K, compared to $\sim 120\mu$K of the temperature anisotropies.

are not physical quantities (i.e. are basis-dependent) and are components of the polarization tensor:

$$\mathcal{P}_{ab}(\hat{n}) = \frac{1}{2}\begin{pmatrix} Q(\hat{n}) & -U(\hat{n})\sin\theta \\ -U(\hat{n})\sin\theta & -Q(\hat{n})\sin^2\theta \end{pmatrix} , \tag{59}$$

in spherical polar coordinates. The electric and magnetic parts of $\mathcal{P}_{ab}$ in equation 58 can be decomposed in spherical harmonics as

$$P_E(\hat{\boldsymbol{n}}) = \sum_{\ell m} \sqrt{\frac{(\ell-2)!}{(\ell+2)!}} a^E_{\ell m} Y_{\ell m}(\hat{\boldsymbol{n}}) , \tag{60}$$

$$P_B(\hat{\boldsymbol{n}}) = \sum_{\ell m} \sqrt{\frac{(\ell-2)!}{(\ell+2)!}} a^B_{\ell m} Y_{\ell m}(\hat{\boldsymbol{n}}) . \tag{61}$$

The separation can be done trivially for full-sky observations. However, ambiguities arise for cut-sky observations as the orthogonality of the E and B tensor harmonics break. Practical methods for performing the separation can be found in, for e.g., [20, 21, 55]. Also [88] have developed multi-scale methods, such as polarized wavelets/curvelets, for the statistical analysis of the polarized maps.

Apart from this extra step, the techniques used in each step of the pipeline presented in the temperature case can be applied to the polarization data. For the polarized data the main diffuse polarized foregrounds are the galactic synchrotron (which is linearly polarized in a uniform magnetic field) and the thermal dust emission (which is linearly polarized if non-spherical grains are aligned in a magnetic field). These emissions have been analyzed for the case of Planck by [34]. At small angular scales extra-galactic radio sources contaminate (equally) to the E- and B-mode power and to remove their effect from the maps one simply excludes the contaminated pixels. Refer to [68] for the application of the ICA method to the polarization data. There is also the PolEMICA [7], which is the application of SMICA to the polarization data. For the maximum-likelihood component separation [92] methods applied to polarization data refer to [90] and [53], where the map making code is called MADAM. In addition, [29] use a Metropolis-within-Gibbs MCMC method for component separation.

For the power spectrum estimation, again, the same methods are applied. For e.g., [59] apply the Gibbs Sampling method to the polarization data. The advantage of the exact methods such as exact likelihood analysis or Gibbs sampling is that they do not suffer from the so-called E-B coupling that exist in methods such as pseudo-C_ℓ methods [85]; the problem arises due to the unorthogonality of the spherical harmonics on a cut-sky, which may cause leakage from the E-mode power into the B-mode power spectrum. Refer to [40] for the a detailed explanation of the pseudo-Cl method . Authors of [55] apply the harmonic ILC (HILC) to estimate the polarization maps and a quadratic estimator approach to estimate the power spectra.

Acknowledgements

This work has been supported by the European Research Council grant SparseAstro (ERC-228261).

References

[1] *Planck: The scientific programme.* 2006.

[2] P. Abrial, Y. Moudden, J.L. Starck, J. Bobin, M.J. Fadili, B. Afeyan, and M.K. Nguyen. Morphological component analysis and inpainting on the sphere: Application in physics and astrophysics. *Journal of Fourier Analysis and Applications*, 13(6), 2007. 729–748.

[3] P. Abrial, Y. Moudden, J.L. Starck, M. J. Fadili, J. Delabrouille, and M. Nguyen. CMB data analysis and sparsity. *Statistical Methodology*, 5(4), 2008. 289-298.

[4] P. Ade, J. Bock, M. Bowden, M. L. Brown, G. Cahill, J. E. Carlstrom, P. G. Castro, S. Church, T. Culverhouse, R. Friedman, K. Ganga, W. K. Gear, J. Hinderks, J. Kovac, A. E. Lange, E. Leitch, S. J. Melhuish, J. A. Murphy, A. Orlando, R. Schwarz, C. O'Sullivan, L. Piccirillo, C. Pryke, N. Rajguru, B. Rusholme, A. N. Taylor, K. L. Thompson, E. Y. S. Wu, and M. Zemcov. First Season QUaD CMB Temperature and Polarization Power Spectra. *APJ*, 674:22–28, February 2008.

[5] N. Aghanim and O. Forni. Searching for the non-Gaussian signature of the CMB secondary anisotropies. *Astronomy and Astrophysics*, 347:409–418, July 1999.

[6] T. Auld, M. Bridges, M. P. Hobson, and S. F. Gull. Fast cosmological parameter estimation using neural networks. *MNRAS*, 376:L11–L15, March 2007.

[7] J. Aumont and J. F. Macías-Pérez. Blind component separation for polarized observations of the cosmic microwave background. *MNRAS*, 376:739–758, April 2007.

[8] A. J. Banday, S. Zaroubi, and K. M. Górski. On the Non-Gaussianity Observed in the COBE Differential Microwave Radiometer Sky Maps. *Astrophysical Journal*, 533, April 2000. 575-587.

[9] L. Bedini, D. Herranz, E. Salerno, C. Baccigalupi, E. E. Kuruouglu, and A. Tonazzini. Separation of correlated astrophysical sources using multiple-lag data covariance matrices. *EURASIP Journal on Applied Signal Processing*, 2005:2400–2412, August 2005.

[10] K. Benabed, J.-F. Cardoso, S. Prunet, and E. Hivon. TEASING: a fast and accurate approximation for the low multipole likelihood of the cosmic microwave background temperature. *MNRAS*, 400:219–227, November 2009.

[11] C. L. Bennett, M. Halpern, G. Hinshaw, N. Jarosik, A. Kogut, M. Limon, S. S. Meyer, L. Page, D. N. Spergel, G. S. Tucker, E. Wollack, E. L. Wright, C. Barnes, M. R. Greason, R. S. Hill, E. Komatsu, M. R. Nolta, N. Odegard, H. V. Peirs, L. Verde, and J. L. Weiland. First year wilkinson microwave anisotropy probe (wmap) observations: Preliminary maps and basic results. *The Astrophysical Journal*, 148:1, 2003.

[12] C. L. Bennett, R. S. Hill, G. Hinshaw, M. R. Nolta, N. Odegard, L. Page, D. N. Spergel, J. L. Weiland, E. L. Wright, M. Halpern, N. Jarosik, A. Kogut, M. Limon, S. S. Meyer, G. S. Tucker, and E. Wollack. First-Year Wilkinson Microwave Anisotropy Probe (WMAP) Observations: Foreground Emission. *APJS*, 148:97–117, September 2003.

[13] F. Bernardeau and J. Uzan. Non-gaussianity in multifield inflation. *PRD*, 66:103506–+, nov 2002.

[14] F. Bernardeau, L. van Waerbeke, and Y. Mellier. Patterns in the weak shear 3-point correlation function. *AAP*, 397, January 2003. 405-414.

[15] E. Bertin and S. Arnouts. SExtractor: Software for source extraction. *Astronomy and Astrophysics, Supplement Series*, 117, June 1996. 393–404.

[16] S. P. Bhavsar and R. J. Splinter. The superiority of the minimal spanning tree in percolation analyses of cosmological data sets. *Monthly Notices of the Royal Astronomical Society*, 282, October 1996. 1461–1466.

[17] A. Bijaoui. Sky background estimation and application. *Astronomy and Astrophysics*, 84, April 1980. 81–84.

[18] J. Bobin, Y. Moudden, J. L. Starck, M.J. Fadili, and N. Aghanim. SZ and CMB reconstruction using generalized morphological component analysis. *Statistical Methodology*, 5(4), 2008. 307–317.

[19] F. R. Bouchet, D. P. Bennett, and A. Stebbins. Patterns of the cosmic microwave background from evolving string networks. *Nature*, 335:410–414, September 1988.

[20] E. F. Bunn, M. Zaldarriaga, M. Tegmark, and A. de Oliveira-Costa. E/B decomposition of finite pixelized CMB maps. *PRD*, 67(2):023501–+, January 2003.

[21] L. Cao and L.-Z. Fang. A Wavelet-Galerkin Algorithm of the E/B Decomposition of Cosmic Microwave Background Polarization Maps. *APJ*, 706:1545–1555, December 2009.

[22] J.-F. Cardoso. Precision cosmology with the cosmic microwave background. *IEEE Signal Processing Magazine*, 27:55–66, January 2010.

[23] P. Carvalho, G. Rocha, and M. P. Hobson. A fast Bayesian approach to discrete object detection in astronomical data sets - PowellSnakes I. *MNRAS*, 393:681–702, March 2009.

[24] P. G. Castro. Bispectrum and the trispectrum of the ostriker-vishniac effect. *PRD*, 67:123001–+, june 2003.

[25] L. Cayón, J. L. Sanz, E. Martínez-González, A. J. Banday, F. Argüeso, J. E. Gallegos, K. M. Górski, and G. Hinshaw. Spherical Mexican hat wavelet: an application to detect non-Gaussianity in the COBE-DMR maps. *Monthly Notices of the Royal Astronomical Society*, 326:1243–1248, October 2001.

[26] P. de Bernardis, P. A. R. Ade, J. J. Bock, J. R. Bond, J. Borrill, A. Boscaleri, K. Coble, B. P. Crill, G. De Gasperis, P. C. Farese, P. G. Ferreira, K. Ganga, M. Giacometti, E. Hivon, V. V. Hristov, A. Iacoangeli, A. H. Jaffe, A. E. Lange, L. Martinis, S. Masi, P. V. Mason, P. D. Mauskopf, A. Melchiorri, L. Miglio, T. Montroy, C. B. Netterfield, E. Pascale, F. Piacentini, D. Pogosyan, S. Prunet, S. Rao, G. Romeo, J. E. Ruhl, F. Scaramuzzi, D. Sforna, and N. Vittorio. A flat Universe from high-resolution maps of the cosmic microwave background radiation. *NAT*, 404:955–959, April 2000.

[27] Jacques Delabrouille, Jean-François Cardoso, and Guillaume Patanchon. Multi–detector multi–component spectral matching and applications for CMB data analysis. *Monthly Notices of the Royal Astronomical Society*, 346(4), December 2003. 1089-1102.

[28] J. Dunkley, A. Amblard, C. Baccigalupi, M. Betoule, D. Chuss, A. Cooray, J. Delabrouille, C. Dickinson, G. Dobler, J. Dotson, H. K. Eriksen, D. Finkbeiner, D. Fixsen, P. Fosalba, A. Fraisse, C. Hirata, A. Kogut, J. Kristiansen, C. Lawrence, A. M. Magalha˜Es, M. A. Miville-Deschenes, S. Meyer, A. Miller, S. K. Naess, L. Page, H. V. Peiris, N. Phillips, E. Pierpaoli, G. Rocha, J. E. Vaillancourt, and L. Verde. Prospects for polarized foreground removal. In S. Dodelson, D. Baumann, A. Cooray, J. Dunkley, A. Fraisse, M. G. Jackson, A. Kogut, L. Krauss, M. Zaldarriaga, & K. Smith , editor, *American Institute of Physics Conference Series*, volume 1141 of *American Institute of Physics Conference Series*, pages 222–264, June 2009.

[29] J. Dunkley, D. N. Spergel, E. Komatsu, G. Hinshaw, D. Larson, M. R. Nolta, N. Odegard, L. Page, C. L. Bennett, B. Gold, R. S. Hill, N. Jarosik, J. L. Weiland, M. Halpern, A. Kogut, M. Limon, S. S. Meyer, G. S. Tucker, E. Wollack, and E. L. Wright. Five-Year Wilkinson Microwave Anisotropy Probe (WMAP) Observations: Bayesian Estimation of Cosmic Microwave Background Polarization Maps. *APJ*, 701:1804–1813, August 2009.

[30] F. -. Dupe, A. Rassat, J. -. Starck, and M. J. Fadili. An Optimal Approach for Measuring the Integrated Sachs-Wolfe Effect. *ArXiv e-prints*, October 2010.

[31] G. Efstathiou. Myths and truths concerning estimation of power spectra: the case for a hybrid estimator. *MNRAS*, 349:603–626, April 2004.

[32] M. Elad, J.-L Starck, D.L. Donoho, and P. Querre. Simultaneous cartoon and texture image inpainting using morphological component analysis (MCA). *Applied and Computational Harmonic Analysis*, 19, 2005. 340–358.

[33] H. K. Eriksen, J. B. Jewell, C. Dickinson, A. J. Banday, K. M. Górski, and C. R. Lawrence. Joint Bayesian Component Separation and CMB Power Spectrum Estimation. *APJ*, 676:10–32, March 2008.

[34] L. Fauvet, J. F. Macías-Pérez, J. Aumont, F. X. Désert, T. R. Jaffe, A. J. Banday, M. Tristram, A. H. Waelkens, and D. Santos. Joint 3D modelling of the polarized Galactic synchrotron and thermal dust foreground diffuse emission. *AAP*, 526:A145+, February 2011.

[35] G. Faÿ, F. Guilloux, M. Betoule, J.-F. Cardoso, J. Delabrouille, and M. Le Jeune. CMB power spectrum estimation using wavelets. *Phys. Rev. D*, 78(8):083013–+, October 2008.

[36] W. A. Fendt and B. D. Wandelt. Pico: Parameters for the Impatient Cosmologist. *APJ*, 654:2–11, January 2007.

[37] D. J. Fixsen, E. Dwek, J. C. Mather, C. L. Bennett, and R. A. Shafer. The Spectrum of the Extragalactic Far-Infrared Background from the COBE FIRAS Observations. *APJ*, 508:123–128, November 1998.

[38] O. Forni and N. Aghanim. Searching for non-gaussianity: Statistical tests. *Astronomy and Astrophysics, Supplement Series*, 137:553–567, June 1999.

[39] B. Gold, N. Odegard, J. L. Weiland, R. S. Hill, A. Kogut, C. L. Bennett, G. Hinshaw, X. Chen, J. Dunkley, M. Halpern, N. Jarosik, E. Komatsu, D. Larson, M. Limon, S. S. Meyer, M. R. Nolta, L. Page, K. M. Smith, D. N. Spergel, G. S. Tucker, E. Wollack, and E. L. Wright.

Seven-year Wilkinson Microwave Anisotropy Probe (WMAP) Observations: Galactic Foreground Emission. *APJS*, 192:15–+, February 2011.

[40] J. Grain, M. Tristram, and R. Stompor. Polarized CMB power spectrum estimation using the pure pseudo-cross-spectrum approach. *PRD*, 79(12):123515–+, June 2009.

[41] A. Gruppuso, A. de Rosa, P. Cabella, F. Paci, F. Finelli, P. Natoli, G. de Gasperis, and N. Mandolesi. New estimates of the CMB angular power spectra from the WMAP 5 year low-resolution data. *MNRAS*, 400:463–469, November 2009.

[42] A. Hajian. Efficient cosmological parameter estimation with Hamiltonian MonteCarlo technique. *PRD*, 75(8):083525–+, April 2007.

[43] D. Herranz and P. Vielva. Cosmic microwave background images. *IEEE Signal Processing Magazine*, 27:67–75, January 2010.

[44] G. Hinshaw et al. Five-Year Wilkinson Microwave Anisotropy Probe (WMAP) Observations:Data Processing, Sky Maps, & Basic Results. 2008.

[45] E. Hivon, K. M. Górski, C. B. Netterfield, B. P. Crill, S. Prunet, and F. Hansen. MASTER of the Cosmic Microwave Background Anisotropy Power Spectrum: A Fast Method for Statistical Analysis of Large and Complex Cosmic Microwave Background Data Sets. *APJ*, 567:2–17, March 2002.

[46] M. P. Hobson, A. W. Jones, and A. N. Lasenby. Wavelet analysis and the detection of non-Gaussianity in the cosmic microwave background. *MNRAS*, 309:125–140, October 1999.

[47] M. P. Hobson and C. McLachlan. A Bayesian approach to discrete object detection in astronomical data sets. *MNRAS*, 338:765–784, January 2003.

[48] A. Hyvärinen, J. Karhunen, and E. Oja. *Independent Component Analysis*. John Wiley, New York, 2001. 481+xxii pages.

[49] M. J. Irwin. Automatic analysis of crowded fields. *Monthly Notices of the Royal Astronomical Society*, 214, June 1985. 575–604.

[50] J. Jewell. A Statistical Characterization of Galactic Dust Emission as a Non-Gaussian Foreground of the Cosmic Microwave Background. *Astrophysical Journal*, 557:700–713, August 2001.

[51] J. Jin, J.-L. Starck, D.L. Donoho, N. Aghanim, and O. Forni. Cosmological non-Gaussian signatures detection: Comparison of statistical tests. *EURASIP Journal*, 15, 2005. 2470–2485.

[52] W. C. Jones, P. A. R. Ade, J. J. Bock, J. R. Bond, J. Borrill, A. Boscaleri, P. Cabella, C. R. Contaldi, B. P. Crill, P. de Bernardis, G. De Gasperis, A. de Oliveira-Costa, G. De Troia, G. di Stefano, E. Hivon, A. H. Jaffe, T. S. Kisner, A. E. Lange, C. J. MacTavish, S. Masi, P. D. Mauskopf, A. Melchiorri, T. E. Montroy, P. Natoli, C. B. Netterfield, E. Pascale, F. Piacentini, D. Pogosyan, G. Polenta, S. Prunet, S. Ricciardi, G. Romeo, J. E. Ruhl, P. Santini, M. Tegmark, M. Veneziani, and N. Vittorio. A Measurement of the Angular Power Spectrum of the CMB Temperature Anisotropy from the 2003 Flight of BOOMERANG. *APJ*, 647:823–832, August 2006.

[53] E. Keihänen, R. Keskitalo, H. Kurki-Suonio, T. Poutanen, and A.-S. Sirviö. Making cosmic microwave background temperature and polarization maps with MADAM. *AAP*, 510:A57+, February 2010.

[54] M. Kilbinger, K. Benabed, O. Cappe, J.-F. Cardoso, G. Fort, S. Prunet, C. P. Robert, and D. Wraith. CosmoPMC: Cosmology Population Monte Carlo. *ArXiv e-prints*, January 2011.

[55] J. Kim, P. Naselsky, and P. R. Christensen. CMB polarization map derived from the WMAP 5year data through the harmonic internal linear combination method. *PRD*, 79(2):023003–+, January 2009.

[56] A. Kogut, D. N. Spergel, C. Barnes, C. L. Bennett, M. Halpern, G. Hinshaw, N. Jarosik, M. Limon, S. S. Meyer, L. Page, G. S. Tucker, E. Wollack, and E. L. Wright. First-Year Wilkinson Microwave Anisotropy Probe (WMAP) Observations: Temperature-Polarization Correlation. *APJS*, 148:161–173, September 2003.

[57] R. G. Kron. Photometry of a complete sample of faint galaxies. *ApJS*, 43:305–325, June 1980.

[58] M. Kunz, A. J. Banday, P. G. Castro, P. G. Ferreira, and K. M. Górski. The Trispectrum of the 4 Year COBE DMR Data. *Astrophysical Journal Letters*, 563:L99–L102, December 2001.

[59] D. L. Larson, H. K. Eriksen, B. D. Wandelt, K. M. Górski, G. Huey, J. B. Jewell, and I. J. O'Dwyer. Estimation of Polarized Power Spectra by Gibbs Sampling. *APJ*, 656:653–660, February 2007.

[60] S. M. Leach, J.-F. Cardoso, C. Baccigalupi, R. B. Barreiro, M. Betoule, J. Bobin, A. Bonaldi, J. Delabrouille, G. de Zotti, C. Dickinson, H. K. Eriksen, J. González-Nuevo, F. K. Hansen, D. Herranz, M. Le Jeune, M. López-Caniego, E. Martínez-González, M. Massardi, J.-B. Melin, M.-A. Miville-Deschênes, G. Patanchon, S. Prunet, S. Ricciardi, E. Salerno, J. L. Sanz, J.-L. Starck, F. Stivoli, V. Stolyarov, R. Stompor, and P. Vielva. Component separation methods for the PLANCK mission. *AAP*, 491, November 2008. 597-615.

[61] E. M. Leitch, J. M. Kovac, N. W. Halverson, J. E. Carlstrom, C. Pryke, and M. W. E. Smith. Degree Angular Scale Interferometer 3 Year Cosmic Microwave Background Polarization Results. *APJ*, 624:10–20, May 2005.

[62] Antony Lewis and Sarah Bridle. Cosmological parameters from cmb and other data: a montecarlo approach. *Physical Review D*, 66:103511, 2002.

[63] Antony Lewis, Anthony Challinor, and Anthony Lasenby. Efficient computation of CMB anisotropies in closed FRW models. *Astrophys. J.*, 538:473–476, 2000.

[64] A. R. Liddle. Statistical Methods for Cosmological Parameter Selection and Estimation. *Annual Review of Nuclear and Particle Science*, 59:95–114, November 2009.

[65] M. Liguori, E. Sefusatti, J. R. Fergusson, and E. P. S. Shellard. Primordial Non-Gaussianity and Bispectrum Measurements in the Cosmic Microwave Background and Large-Scale Structure. *Advances in Astronomy*, 2010, 2010.

[66] M. López-Caniego, J. González-Nuevo, D. Herranz, M. Massardi, J. L. Sanz, G. De Zotti, L. Toffolatti, and F. Argüeso. Nonblind Catalog of Extragalactic Point Sources from the Wilkinson Microwave Anisotropy Probe (WMAP) First 3 Year Survey Data. *ApJS*, 170:108–125, May 2007.

[67] M. Lopez-Caniego, D. Herranz, R. B. Barreiro, and J. L. Sanz. Some comments on the note "Some comments on the paper 'Filter design for the detection of compact sources based on the Neyman-Pearson detector' by M. Lopez-Caniego et. al (2005, MNRAS 359, 993)" by R. Vio and P. Andreani (astroph/0509394). *ArXiv Astrophysics e-prints*, September 2005.

[68] D. Maino, S. Donzelli, A. J. Banday, F. Stivoli, and C. Baccigalupi. CMB signal in WMAP 3yr data with FastICA. *ArXiv Astrophysics e-prints*, September 2006.

[69] J.-B. Melin, J. G. Bartlett, and J. Delabrouille. Catalog extraction in SZ cluster surveys: a matched filter approach. *A&A*, 459:341–352, November 2006.

[70] T. E. Montroy, P. A. R. Ade, J. J. Bock, J. R. Bond, J. Borrill, A. Boscaleri, P. Cabella, C. R. Contaldi, B. P. Crill, P. de Bernardis, G. De Gasperis, A. de Oliveira-Costa, G. De Troia, G. di Stefano, E. Hivon, A. H. Jaffe, T. S. Kisner, W. C. Jones, A. E. Lange, S. Masi, P. D. Mauskopf, C. J. MacTavish, A. Melchiorri, P. Natoli, C. B. Netterfield, E. Pascale, F. Piacentini, D. Pogosyan, G. Polenta, S. Prunet, S. Ricciardi, G. Romeo, J. E. Ruhl, P. Santini, M. Tegmark, M. Veneziani, and N. Vittorio. A Measurement of the CMB <EE> Spectrum from the 2003 Flight of BOOMERANG. *APJ*, 647:813–822, August 2006.

[71] Y. Moudden, J. f. Cardoso, J. l. Starck, and J. Delabrouille. Blind component separation in wavelet space: Application to cmb analysis. *EURASIP Journal on Applied Signal Processing*, 2005:2437–2454, 2005.

[72] A. A. Penzias and R. W. Wilson. A Measurement of Excess Antenna Temperature at 4080 Mc/s. *APJ*, 142:419–421, July 1965.

[73] L. Perotto, J. Bobin, S. Plaszczynski, J. -. Starck, and A. Lavabre. Reconstruction of the CMB lensing for Planck. *ArXiv e-prints*, March 2009.

[74] Planck Collaboration, P. A. R. Ade, N. Aghanim, M. Arnaud, M. Ashdown, J. Aumont, C. Baccigalupi, A. Balbi, A. J. Banday, R. B. Barreiro, and et al. Planck Early Results: The Early Release Compact Source Catalog. *ArXiv e-prints*, January 2011.

[75] N. Ponthieu, J. F. Macías-Pérez, M. Tristram, P. Ade, A. Amblard, R. Ansari, J. Aumont, É. Aubourg, A. Benoît, J.-P. Bernard, A. Blanchard, J. J. Bock, F. R. Bouchet, A. Bourrachot, P. Camus, J.-F. Cardoso, F. Couchot, P. de Bernardis, J. Delabrouille, F.-X. Désert, M. Douspis, L. Dumoulin, P. Filliatre, P. Fosalba, M. Giard, Y. Giraud-Héraud, R. Gispert, J. Grain, L. Guglielmi, J.-C. Hamilton, S. Hanany, S. Henrot-Versillé, J. Kaplan, G. Lagache, A. E. Lange, K. Madet, B. Maffei, S. Masi, F. Mayet, F. Nati, G. Patanchon, O. Perdereau, S. Plaszczynski, M. Piat, S. Prunet, J.-L. Puget, C. Renault, C. Rosset, D. Santos, D. Vibert, and D. Yvon. Temperature and polarization angular power spectra of Galactic dust radiation at 353 GHz as measured by Archeops. *AAP*, 444:327–336, December 2005.

[76] W. H. Press, S. A. Teukolsky, W. T. Vetterling, and B. P. Flannery. *Numerical recipes in FORTRAN. The art of scientific computing.* 1992.

[77] H. Rauhut and R. Ward. Sparse Legendre expansions via ℓ_1 minimization. *ArXiv e-prints*, March 2010.

[78] A. C. S. Readhead, B. S. Mason, C. R. Contaldi, T. J. Pearson, J. R. Bond, S. T. Myers, S. Padin, J. L. Sievers, J. K. Cartwright, M. C. Shepherd, D. Pogosyan, S. Prunet, P. Altamirano, R. Bustos, L. Bronfman, S. Casassus, W. L. Holzapfel, J. May, U.-L. Pen, S. Torres, and P. S. Udomprasert. Extended Mosaic Observations with the Cosmic Background Imager. *APJ*, 609:498–512, July 2004.

[79] A. Riazuelo, J.-P. Uzan, R. Lehoucq, and J. Weeks. Simulating cosmic microwave background maps in multi-connected spaces. astro-ph/0212223, 2002.

[80] G. Rocha, C. R. Contaldi, J. R. Bond, and K. M. Gorski. Application of XFaster power spectrum and likelihood estimator to Planck. *ArXiv e-prints*, December 2009.

[81] M. Sato, K. Ichiki, and T. T. Takeuchi. Precise Estimation of Cosmological Parameters Using a More Accurate Likelihood Function. *Physical Review Letters*, 105(25):251301–+, December 2010.

[82] D. Scott, J. Silk, and M. White. From Microwave Anisotropies to Cosmology. *Science*, 268:829–835, May 1995.

[83] U. Seljak and M. Zaldarriaga. A Line-of-Sight Integration Approach to Cosmic Microwave Background Anisotropies. *APJ*, 469:437–+, October 1996.

[84] S. F. Shandarin. Testing non-Gaussianity in cosmic microwave background maps by morphological statistics. *Monthly Notices of the Royal Astronomical Society*, 331:865+, April 2002.

[85] K. M. Smith. Pure pseudo-C_l estimators for CMB B-modes. *NAR*, 50:1025–1029, December 2006.

[86] G. F. Smoot, C. L. Bennett, A. Kogut, E. L. Wright, J. Aymon, N. W. Boggess, E. S. Cheng, G. de Amici, S. Gulkis, M. G. Hauser, G. Hinshaw, P. D. Jackson, M. Janssen, E. Kaita, T. Kelsall, P. Keegstra, C. Lineweaver, K. Loewenstein, P. Lubin, J. Mather, S. S. Meyer, S. H. Moseley, T. Murdock, L. Rokke, R. F. Silverberg, L. Tenorio, R. Weiss, and D. T. Wilkinson. Structure in the COBE differential microwave radiometer first-year maps. *APJ*, 396:L1–L5, September 1992.

[87] J.-L. Starck, N. Aghanim, and O. Forni. Detecting cosmological non-Gaussian signatures by multi-scale methods. *Astronomy and Astrophysics*, 416, 2004. 9–17.

[88] J.-L. Starck, Y. Moudden, and J. Bobin. Polarized wavelets and curvelets on the sphere. *AAP*, 497:931–943, April 2009.

[89] J.-L. Starck, F. Murtagh, and M.J. Fadili. *Sparse Image and Signal Processing.* Cambridge University Press, 2010.

[90] F. Stivoli, J. Grain, S. M. Leach, M. Tristram, C. Baccigalupi, and R. Stompor. Maximum likelihood, parametric component separation and CMB B-mode detection in suborbital experiments. *MNRAS*, 408:2319–2335, November 2010.

[91] V. Stolyarov, M. P. Hobson, A. N. Lasenby, and R. B. Barreiro. All-sky component separation in the presence of anisotropic noise and dust temperature variations. *MNRAS*, 357:145–155, February 2005.

[92] R. Stompor, S. Leach, F. Stivoli, and C. Baccigalupi. Maximum likelihood algorithm for parametric component separation in cosmic microwave background experiments. *MNRAS*, 392:216–232, January 2009.

[93] R. A. Sunyaev and I. B. Zeldovich. Microwave background radiation as a probe of the contemporary structure and history of the universe. *Annual Review of Astronomy and Astrophysics*, 18, 1980. 537-560.

[94] R. A. Sunyaev and Y. B. Zeldovich. The Observations of Relic Radiation as a Test of the Nature of X-Ray Radiation from the Clusters of Galaxies. *Comments on Astrophysics and Space Physics*, 4:173–+, November 1972.

[95] I. Szapudi, S. Prunet, and S. Colombi. Fast Clustering Analysis of Inhomogeneous Megapixel CMB maps. *ArXiv Astrophysics e-prints*, July 2001.

[96] M. Tristram, J. F. Macías-Pérez, C. Renault, and D. Santos. XSPECT, estimation of the angular power spectrum by computing cross-power spectra with analytical error bars. *MNRAS*, 358:833–842, April 2005.

[97] L. Verde, H. V. Peiris, D. N. Spergel, M. R. Nolta, C. L. Bennett, M. Halpern, G. Hinshaw, N. Jarosik, A. Kogut, M. Limon, S. S. Meyer, L. Page, G. S. Tucker, E. Wollack, and E. L. Wright. First-Year Wilkinson Microwave Anisotropy Probe (WMAP) Observations: Parameter Estimation Methodology. *APJS*, 148:195–211, September 2003.

[98] D. Wraith, M. Kilbinger, K. Benabed, O. Cappé, J.-F. Cardoso, G. Fort, S. Prunet, and C. P. Robert. Estimation of cosmological parameters using adaptive importance sampling. *PRD*, 80(2):023507–+, July 2009.

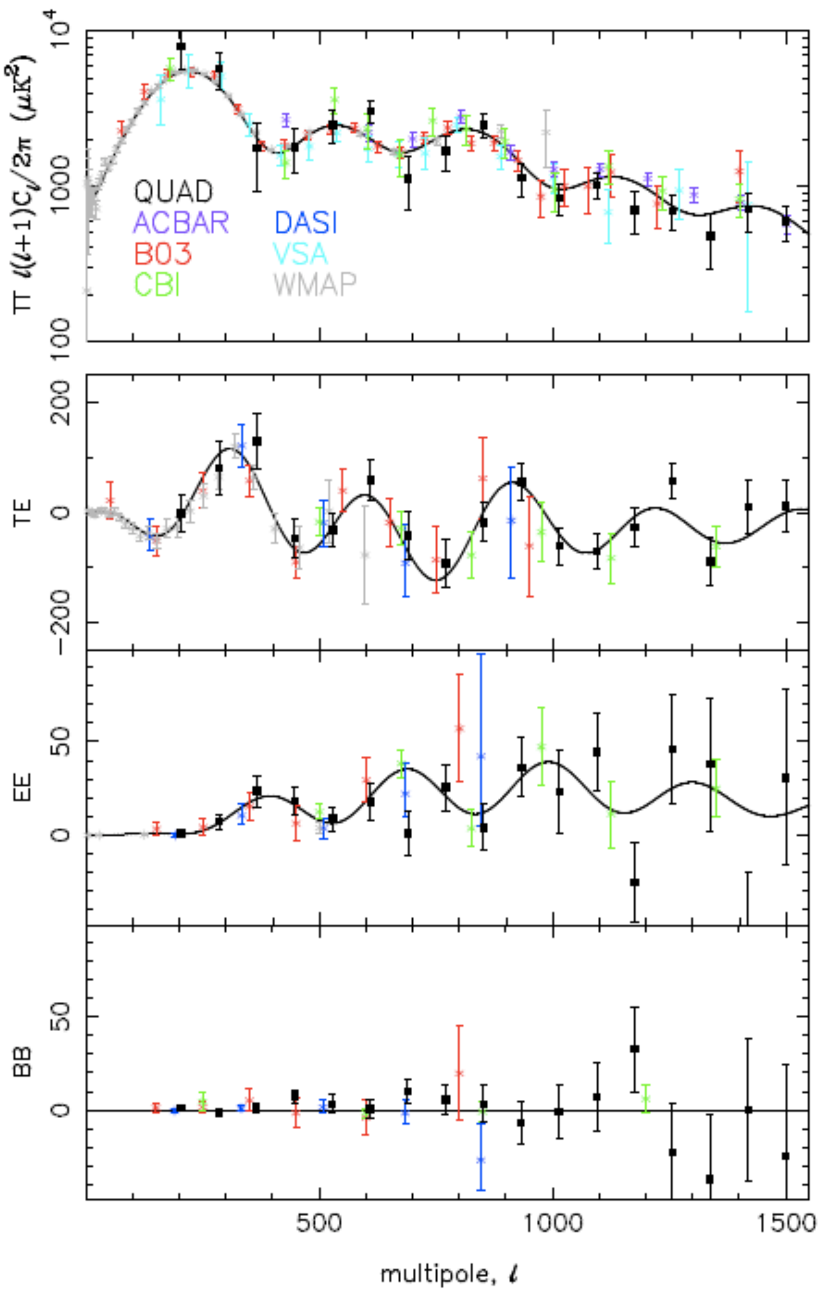

Figure 4: CMB temperature and polarization power spectra measured by different CMB experiments, each covering different range of scales [4].